

MS No.: acp-2019-123

Title: *Exploiting multi-wavelength aerosol absorption coefficients in a multi-time resolution source apportionment study to retrieve source-dependent absorption parameters*

Authors: Alice C. Forello et al.

Response to Reviewers

The authors acknowledge reviewers for their comments and suggestions, which helped the authors in improving the paper. The authors changed text and figures according to the concerns raised by all referees. English language and grammar was thoroughly revised.

RESPONSE TO REVIEWER 1

R1-1. This is a paper which succeeds in combining two areas of investigation in a rather successful way. It takes multi-component chemical data from atmospheric aerosol collected in Milan and processes it together with multi-wavelength optical absorption data in a single analysis using the multi-linear engine ME-2. As well as successfully combining two different kinds of data with different metrics, which has been done before but not for these specific metrics (more usually for particle mass and number size distribution data), it also successfully combines data measured over different averaging periods. The latter is not entirely novel but there are only a small number of earlier reports in the literature. Consequently, this is advanced receptor modelling work which shows both how using the multi-wavelength optical absorption data from an aethalometer can strengthen source apportionment of light-absorbing components and also that the data can be used in reverse to estimate the optical properties of particles from specific sources.

A1-1. *It is worth noting that the approach here presented is of general interest as (1) in this work optical data were retrieved by a home-made multi-wavelength polar photometer but – as underlined by the Referee - the methodology here presented could be applied to datasets combining aerosol chemical and optical data obtained by widespread instrumentation (e.g. Aethalometers for optical data); (2) input data to the receptor model not necessarily should comprise variables acquired with different time resolution as we did here. We added a sentence on the general character of our work in the revised version of the paper (see lines 38-40 in the abstract and 106-110 afterwards).*

R1-2. The paper is in general well written although some aspects of the English could be improved. My main criticism of the science is the lack of detail over the methods. For example, the procedures appear to be successful in combining elemental data and optical absorption data with entirely different metrics and yet outputting concentrations and explained variation for both types of constituent in their original units. This has previously posed problems for PMF but presumably also for ME-2.

A1-2. *ME-2/PMF analysis is not a-priori harmed by the use of joint matrices containing different units, as we ascertained after having studied a number of published papers/users' guides before joining optical and chemical data in the same input matrix. Recently, this point has been also extensively discussed and explained by P. Paatero in an open discussion on ACPD (see <https://doi.org/10.5194/acp-2018-784-RC2>). Indeed, as he stated, if different units are present in different columns of matrix X , the output data in factor matrix G are pure numbers and elements in a column of factor matrix F carry the same dimension and unit as the original data in matrix X . In*

addition, as we did in this work, the average total contribution to the mass of a specific source due to species in a certain factor in matrix F must be retrieved a-posteriori summing up only mass contributions by chemical components (i.e. excluding optical components in matrix F).

Following the Referee's comment, we decided to add a short sentence about this point which is often considered an issue in PMF/ME analysis but it is mainly due to a misunderstanding (see lines 302-307 in the revised version).

R1-3. Secondly, there is no information on whether an error matrix was constructed, and if so, how this was carried out. There are fairly widely accepted methods for chemical data, but how was this achieved for the optical absorption data?

A1-3. *In the revised version of the paper, we added experimental uncertainties and MDLs (as reported for each analysis in sections 2.2 and 2.3) and some sentences hopefully clarify how uncertainties were handled in the model. See e.g.*

Lines 138-140: In this Section, chemical analyses performed on samples are summarised. As measured concentration in each sample was characterised by its own uncertainty, only ranges for experimental uncertainties and minimum detection limits (MDLs) for every set of variables are reported.

Lines 168-171: PM10 hourly concentrations of most elements and samples were characterised by relative uncertainties in the range 10-30% (higher uncertainties for elements near MDL) and MDLs ranged from a minimum of 0.1 to a maximum of 2.5 ng m⁻³ (higher MDLs typically detected for Z<20 elements).

Lines 198-201: Uncertainties on b_{ap} were estimated as 15 % and MDL was in the range 1-10 Mm⁻¹ depending on sampling duration and wavelength as already reported in our previous works (Vecchi et al., 2014; Bernardoni et al., 2017c). Experimental uncertainties and MDL of optical absorption data were used as a starting point to estimate the uncertainties introduced in the model. Pre-treatment procedure for these data was the same used for chemical variables (see also Sect. 2.5).

Lines 269-273: Every measured variable in each sample is characterised by its own uncertainty; ranges of experimental uncertainties and MDLs are reported in Sect. 2.2 and 2.3 for chemical and optical analyses, respectively. Variables with more than 20 % of the concentration data below MDL values were omitted from the analysis (Ogulei et al., 2005). The procedure described in Polissar et al. (1998) was followed to treat uncertainties and below MDL data, starting from experimental uncertainties and MDLs.

Lines 288-291: The input matrix X consisted in 386 samples and the total number of time units was 1117. The analysis was performed in the robust mode; lower limit for G contribution was set to -0.2 (Brown et al., 2015) and the error model $em=-14$ was used for the main equation with $C1=$ input error, $C2= 0.0$ and $C3=0.1$ (Paatero, 2012) for both chemical and optical absorption data.

R1-4. The assignment of identity to the eight factors output by the ME-2 looks very reasonable but there are some specific points that are not addressed. The sulphate factor contains a higher concentration of organic carbon than of sulphur and possibly a higher concentration of organic matter than sulphate (although this is not possible to read from the graph).

A1-4. *The concern raised by the Referee was addressed discussing a bit further this point in the revised text (see lines 391-404): "The factor associated to sulphate shows EVF=0.47 for S and much lower EVF for all the other variables in the factor. Considering the contribution of S in the chemical profile in terms of sulphate and ammonium sulphate, the relative contribution of sulphur components*

in the profile increases from 11% (S) up to 45% (ammonium sulphate). The latter is the main sulphur compound detected in the Po valley as reported in previous papers such as e.g. Marcazzan et al. (2001) and was by far the highest contributor in the chemical profile. The other important contributor was OC (19%), whose impact on PM mass increased up 30% when reported as organic matter using 1.6 as the organic carbon-to-organic matter conversion factor for this site (Vecchi et al., 2004). Due to the secondary origin of the aerosol associated to this factor, it was not surprising to find also a significant OC contribution; indeed, aerosol chemical composition in Milan is impacted by highly oxygenated components due to aging processes favoured by strong atmospheric stability (Vecchi et al., 2018 and 2019). In this factor, EC contributed for about 1%. Considering the total EC concentration reconstructed by the model, the EC fraction related to the sulphate factor was about 6%. Opposite to sulphates, EC has a primary origin; however, its presence with a very similar percentage (4-5%) in a sulphate chemical profile was previously pointed out in Milan, indicating a more complex mixing between primary and secondary sources (Amato et al., 2016). The sulphate factor accounted for 21 % of the PM10 mass.”

R1-5. No mention is made of this organic matter which accounts for a significant proportion of the explained variation of the optical absorption. Presumably this is secondary organic matter correlated with sulphate, but does it have light absorbing properties which are of interest? As various workers have pointed out, this creates problems for the two component “aethalometer” model widely used for source apportionment of wood smoke (but which is not in itself a problem for the ME-2 method). The resuspended dust also appears to have some optical absorption. Could this be associated with the iron minerals?

A1-5. *To address the Referee’s concern, in the revised text we discussed a bit more results related to the other contributors to aerosol absorption in atmosphere although their contribution is not significant in terms of EVF (ranging from 0.08 to 0.12 for sulphate and from 0.03 to 0.06 for resuspended dust, depending on the wavelength).*

Lines 497-508: “The third contributor to aerosol absorption in atmosphere was the sulphate factor, with a contribution comparable to the biomass burning one at 780 nm (about 20% of the total reconstructed bap at this wavelength). The sulphate factor contained a small fraction of EC, as previously discussed (see Sect. 3.2). This might be explained considering that non/weakly light-absorbing material can form a coating able to enhance absorption (Bond & Bergstrom, 2006; Fuller et al., 1999) within a few days after emission (Bond et al., 2006). Laboratory experiments and simulations from in-situ measurements highlighted absorption amplification for absorbing particles coated with secondary organic aerosol (Schnaiter et al., 2003; Moffet & Prather, 2009). These processes related to particles aging can become important in the Po valley due to low atmospheric dispersion conditions and they might explain the relatively high contribution of the sulphate factor to the absorption coefficient in respect to the other sources (excluding traffic and biomass burning). Among the other sources, resuspended dust was the main contributor at all wavelengths (between 3% and 7% of the total reconstructed bap, depending on the wavelength), likely due to the role of iron minerals. The other four sources were less relevant in terms of EVF values and overall contributed for less than 11%.”

R1-6. The aged sea salt factor contains substantially more sulphate than sodium and unusually absolutely no nitrate. Although it is shown that the temporal variation of this factor correlates with

that of chloride, it appears that this factor is very atypical of aged sea salt and may well be mixed with other components.

A1-6. *The Referee is right, being Milan about 120 km far from the nearest coast, when occasionally observed, transported marine air masses are affected by the pollution encountered in the Po valley. This is why the chemical profile of this aged sea salt is dirty and clearly mixed with other components. Nevertheless, this feature is expected and can be explained considering that during air mass transport from the sea to continental polluted areas sodium chloride can react with sulfuric acid vapor, producing sodium sulphate and hydrochloric acid vapor and giving chloride depletion (Seinfeld and Pandis, 2006). As the Referee points out, chloride deficit can also be caused by NaCl reacting with HNO₃ and producing NaNO₃ in particulate phase (Seinfeld and Pandis, 2006). The presence of nitrate and sulphate in aged sea salt chemical profile has been previously reported for a number of sites e.g. by Amato et al. (2016), including also Milan.*

The aged sea salt source is enriched in sulphate even though its share in this factor is low compared to its overall concentration in PM (10% of the total reconstructed variable). As for the lack of nitrate, following Lee et al. (1999) a very rough estimate of the NO₃⁻ content that can be ascribed to this factor is from 0% to a maximum of 2% (about 82 ng m⁻³) of the total reconstructed concentration of NO₃⁻ in atmosphere, that can be considered totally negligible compared to changes in the mass contribution of sources of NO₃⁻. From the experimental data, it is not possible to obtain information about nitrate transport during marine mass advection: atmospheric concentrations of NO₃⁻ over 12 or 24 hours comprising the marine advection are always very low, because of “cleaner” air mass (255 ng m⁻³ in summer and 1.4 µg m⁻³ in winter, to be compared with average values during the two seasons of 1.4 µg m⁻³ and 9.0 µg m⁻³, respectively). It is possible that NO₃⁻ measurements available only at low-time resolution influence its estimation in the aged sea salt episodic source. Anyway, the multi-time model was able to catch the signal and the main tracers of this episodic source.

We added a sentence, at lines 447-451: “When marine air masses are transported to polluted sites, sea salt particles are characterised by a Cl deficit due to reactions with sulphuric and nitric acid (Seinfeld and Pandis, 2006). In this case, the factor chemical profile was expected to be enriched in sulphate and nitrate. In this work, nitrate was not present; a very rough estimate (Lee et al., 1999) gave a maximum expected contribution of 2 % (about 82 ng m⁻³) of the total nitrate mass in atmosphere, that can be considered negligible in terms of mass contribution of the sources.”

R1-7. The derivation of Ångström coefficients from the apportioned optical absorption data is interesting but there is little comment on the fact that the value for fossil fuel is 0.78 to 0.88 (25th-75th percentile) which extends slightly below the range of typically reported values and is distinctly different from the value of 1.0 used by most workers in the “aethalometer” model. The value of Ångström coefficients for the biomass burning factor is well within the very wide range of literature values which depend very much upon combustion conditions and is a useful addition to the literature, as are the estimated mass absorption cross-sections.

A1-7. *There is an open discussion on the “best” α value to be used in the Aethalometer model as for fossil fuel as in the literature it ranges from 0.8-1.1 (see e.g. Sandradewi et al., 2008 and Zotter et al., 2017). Indeed, $\alpha_{FF}=1$ is derived from the theory of absorption of spherical particles in the Rayleigh regime, but both experimental and modelling studies highlighted the possibility to have also lower values for atmospheric particles due to the influence of particle size distribution and aging processes in atmosphere (as reported at lines 542-545). In addition, in this work aerosol absorption coefficient at different wavelengths is measured on PTFE and polycarbonate filters (i.e. membranes),*

while reported literature values are usually retrieved from filter-based instrumentation using fibre-filter tapes, which are known to be affected by possible biases. We reported this issue at lines 184-188: “Moreover, previous works reported a bias on b_{ap} measured by instrumentation using fibre filters (e.g. Cappa et al., 2008; Lack et al., 2008; Davies et al., 2019; and references therein); Vecchi et al. (2014) quantified in about 40% the effect caused in b_{ap} values (assessed at 635 nm) by sampling artefacts due to organics in aerosol samples collected in Milan when comparing aerosol samples collected in parallel quartz-fibre and PTFE filters.”.

In addition to addressing the points above, there are two lesser issues which should be considered.

(a) Line 254 – the intercept requires the units to be meaningful.

Absolutely right, it has been added.

(b) Line 307 – it is stated that “in the factor interpreted as nitrate the explained variation is fully ascribed to NO_3^- ”. Would it not be more correct to state that the nitrate factor accounts for 100% of the explained variation in NO_3^- ?

Yes, indeed. It has been corrected in the revised version (line 382) as follows: “The factor interpreted as nitrate fully accounted for the explained variation of NO_3^- .”

References

- Amato et al. (2016). AIRUSE-LIFE+: a harmonized PM speciation and source apportionment in five southern European cities. *Atmos. Chem. Phys.*, 16, 3289–3309.
- Cappa C.D., Lack D.A., Burkholder J.B., and Ravishankara A.R.: Bias in filter-based aerosol light absorption measurements due to organic aerosol loading: Evidence from laboratory measurements. *Aerosol Sci. Tech.*, 42, 1022-1032.
- Davies N.W., Fox C., Szpek K., Cotterell M.I., Taylor J.W., Allan J.D., Williams P.I., Trembath J., Haywood J.M., and Langridge J.M.: Evaluating biases in filter-based aerosol absorption measurements using photoacoustic spectroscopy, *Aerosol Meas. Tech.*, 12, 3417–3434.
- Lack D.A., Cappa C.D., Covert D.S., Baynard T., Massoli P., Sierau B., Bates T.S., Quinn P.K., Lovejoy E.R., and Ravishankara A.R.: Bias in filter-based aerosol light absorption measurements due to organic aerosol loading: Evidence from ambient measurements. *Aerosol Sci. Tech.*, 42, 1033-1041.
- Marcazzan et al. (2001). Characterisation of PM10 and PM2.5 particulate matter in the ambient air of Milan (Italy), *Atmos. Environ.*, 35, 4639-4650.
- Paatero P. (2018). Open discussion on ACPD at <https://doi.org/10.5194/acp-2018-784-RC2>
- Sandradewi J., Prévôt A.S.H., Szidat S., Perron N., Alfarra M.R., Lanz V.A., Weingartner E. and Baltensperger U.: Using aerosol light absorption measurements for the quantitative determination of wood burning and traffic emission contributions to particulate matter, *Environ. Sci. Technol.*, 42, 3316-3323, 2008a.
- Seinfeld J.H. and Pandis S.N. (2006): *Atmospheric chemistry and physics: from air pollution to climate change*, 2nd edition, John Wiley & Sons, INC, Hoboken, New Jersey.
- Vecchi R., Bernardoni V., Paganelli C. and Valli G.: A filter-based light absorption measurement with polar photometer: effects of sampling artefacts from organic carbon, *J. Aerosol. Sci.*, 70, 15-25, <https://doi.org/10.1016/j.jaerosci.2013.12.012>, 2014.
- Zotter P., Herich H., Gysel M., El-Haddad I., Zhang Y., Mocnik G., Hüglin C., Baltensperger U., Szidat S. and Prévôt A.S.H.: Evaluation of the absorption Ångström exponents for traffic and wood burning in the Aethalometer-based source apportionment using radiocarbon measurements of ambient aerosol, *Atmos. Chem. Phys.*, 17, 4229-4249, <https://doi.org/10.5194/acp-17-4229-2017>, 2017.

RESPONSE TO REVIEWER 2

R2-1. This article presents a source apportionment analysis within the urban area of Milan, Italy. The originality of this study firstly lies in the use of data with different temporal resolutions as one single input data. A modified equation of the standard equation of the Multilinear Engine has been used, which has been scarcely used in the literature. The second original feature is the use of absorption data. The authors were therefore able to derive optical properties of the obtained factors. Overall, the paper is well-written and is well-organized. I think it deserves publication in ACP, but several points need to be addressed before.

I fully agree with reviewer #1 about the methods section. The authors need to be much more didactic on the way they handled uncertainties: - First, little information is provided regarding the calculation of uncertainties for each variable. Sometimes a range of values is provided, but we don't know which value was actually used with the Polissar equation.

A2-1 *In the revised version of the paper, we added experimental uncertainties and MDL (as reported for each analysis in sections 2.2 and 2.3) and some sentences hopefully clarify how uncertainties were handled in the model. See e.g.*

Lines 138-140: In this Section, chemical analyses performed on samples are summarised. As measured concentration in each sample was characterised by its own uncertainty, only ranges for experimental uncertainties and minimum detection limits (MDLs) for every set of variables are reported.

Lines 168-171: PM10 hourly concentrations of most elements and samples were characterised by relative uncertainties in the range 10-30% (higher uncertainties for elements near MDL) and MDLs ranged from a minimum of 0.1 to a maximum of 2.5 ng m⁻³ (higher MDLs typically detected for Z<20 elements).

Lines 198-201: Uncertainties on b_{ap} were estimated as 15 % and MDL was in the range 1-10 Mm⁻¹ depending on sampling duration and wavelength as already reported in our previous works (Vecchi et al., 2014; Bernardoni et al., 2017c). Experimental uncertainties and MDL of optical absorption data were used as a starting point to estimate the uncertainties introduced in the model. Pre-treatment procedure for these data was the same used for chemical variables (see also Sect. 2.5).

Lines 269-273: Every measured variable in each sample is characterised by its own uncertainty; ranges of experimental uncertainties and MDLs are reported in Sect. 2.2 and 2.3 for chemical and optical analyses, respectively. Variables with more than 20 % of the concentration data below MDL values were omitted from the analysis (Ogulei et al., 2005). The procedure described in Polissar et al. (1998) was followed to treat uncertainties and below MDL data, starting from experimental uncertainties and MDLs.

Lines 288-291: The input matrix X consisted in 386 samples and the total number of time units was 1117. The analysis was performed in the robust mode; lower limit for G contribution was set to -0.2 (Brown et al., 2015) and the error model $em=-14$ was used for the main equation with $C1=$ input error, $C2= 0.0$ and $C3=0.1$ (Paatero, 2012) for both chemical and optical absorption data.

R2-2. Also, since absorption data are rarely used in PMF analyses, I would recommend to perform sensitivity tests on the uncertainty of 15% that was used, and evaluate the impact on the PMF results.

A2-2. *Sensitivity tests on the uncertainty of absorption data were performed starting from a minimum uncertainty of 10%. Lower uncertainties were considered not physically meaningful from an experimental point of view. ME-2 analyses performed with this minimum uncertainty on absorption*

data gave very similar results to the base case solution presented in the Supplement (Figure S1 and Table S1), with no differences in mass apportionment and a maximum variation in the concentrations of chemical and optical profiles (matrix F) of 7% considering significant variables in each profile (EVF higher or near 0.30). Opposite, with an uncertainty of 20% on absorption data, the solution corresponding to the minimum Q value was different from the base case one presented in the Supplement. The factors assigned to resuspended dust and construction works got mixed, and a new unique factor (traced almost exclusively by Pb) appeared, with mass contribution equal to zero. A quantitative parameter to estimate how much chemical and optical variables “drive” the model is the “Total weight”, recently introduced by P. Paatero in an open discussion on ACPD about joint analyses of matrices of variables with different units (see <https://doi.org/10.5194/acp-2018-784-RC2>).

In our work, 18 chemical variables and 4 optical variables were introduced in the multi-time resolution model (see section 2.5) and the ratio between the total weight of the “chemical variables matrix” and the “optical variables matrix” was about 9, 12, and 19 considering an uncertainty on absorption data of 10%, 15%, and 20%, respectively.

In this case, it seems that when the “chemical variables matrix” weights about 19 times more than the optical matrix, it drives the model too much (i.e. relevance of optical variables is weakened and no useful information are added by the joint datasets); opposite, a ratio of 12 is enough to avoid any variable-driven solution. The ratios obtained for a joint analysis of chemical and optical variables clearly depend on the variables used, the matrices dimension and the parameters implemented in the model; more studies are needed to give more robust indication on the “optimum” ratio for this kind of analyses.

In conclusion, we considered the experimental uncertainty of 15% as the best option for our optical absorption data. A comment on sensitivity tests results is now reported at lines 292-301.

R2-3. Then, the reader has no information about the balance of the Q in the input variables, yet being a critical issue in the multi-time algorithm. Have the authors adjusted the uncertainties so that the Q is approximately balanced in each group of variables?

A2-3. *Obviously, the number of variables in each time frame will contribute different amounts to the Q. Variables with higher time resolution have more values so they influence Q more than the lower time resolution variables. That is the whole point of the approach. We know that there is more potential for edge points in the high time resolution data since we are not averaging over higher and lower concentrations in the longer time periods. Thus, we want there to be imbalanced in the Q so that the data with the maximum source information drives the solution and those data are the higher time resolution data.*

To the authors’ knowledge there is no literature papers on multi-time resolution ME-2 where different portions of the Q are weighed so that the variables with different time resolutions have equal impact on the solution. That would defeat the purpose of using the data in their native time resolutions.

In some models, where there is an auxiliary Q, you want it to have less weight than the main Q, but in the Q itself, you really do not want to start fooling with weighting groups of variables.

The authors would like to acknowledge P. Hopke, who shared his expertise with us about this point.

R2-4. The authors state that scaled residuals are randomly distributed between -3 and 3. Are these residuals centered around 0, with a Gaussian shape?

A2-4. *The Referee is right, we forgot to comment on the shape of scaled residuals distribution. For each variable, the scaled residuals of the base case solution are now reported in the Supplement (Fig. S2). In addition, at lines 357-359 a sentence was added “with a Gaussian shape for most of the variables (Fig. S2 in the Supplement).”*

R2-5. I am also a bit disappointed to see that discussions about optical properties are essentially focused on traffic and wood-burning, but little is said about absorption found in the nitrate-rich factor, the sulfate-rich factor (the presence of EC in the profile is not discussed) and the dust factor.

A2-5. *We decided to focus the discussion about optical properties specifically on fossil fuel and biomass burning, in order to be comparable to the approach of the widespread Aethalometer model, as mentioned at lines 519-522.*

To address the Referee’s concern, in the revised text we discussed a bit more results related to the other contributors to aerosol absorption in atmosphere although their contribution is not significant in terms of EVF (ranging from 0.08 to 0.12 for sulphate and from 0.03 to 0.06 for resuspended dust, depending on the wavelength).

Lines 497-508: “The third contributor to aerosol absorption in atmosphere was the sulphate factor, with a contribution comparable to the biomass burning one at 780 nm (about 20% of the total reconstructed b_{ap} at this wavelength). The sulphate factor contained a small fraction of EC, as previously discussed (see Sect. 3.2). This might be explained considering that non/weakly light-absorbing material can form a coating able to enhance absorption (Bond & Bergstrom, 2006; Fuller et al., 1999) within a few days after emission (Bond et al., 2006). Laboratory experiments and simulations from in-situ measurements highlighted absorption amplification for absorbing particles coated with secondary organic aerosol (Schnaiter et al., 2003; Moffet & Prather, 2009). These processes related to particles aging can become important in the Po valley due to low atmospheric dispersion conditions and they might explain the relatively high contribution of the sulphate factor to the absorption coefficient in respect to the other sources (excluding traffic and biomass burning). Among the other sources, resuspended dust was the main contributor at all wavelengths (between 3% and 7% of the total reconstructed b_{ap} , depending on the wavelength), likely due to the role of iron minerals. The other four sources were less relevant in terms of EVF values and overall contributed for less than 11%.”

About the presence of EC in the sulphate factor, we added a little discussion in the paragraph regarding this factor.

See lines 400-403: “In this factor, EC contributed for about 1%. Considering the total EC concentration reconstructed by the model, the EC fraction related to the sulphate factor was about 6%. Opposite to sulphates, EC has a primary origin; however, its presence with a very similar percentage (4-5%) in a sulphate chemical profile was previously pointed out in Milan, indicating a more complex mixing between primary and secondary sources (Amato et al., 2016).”

R2-6. Finally, in order to strengthen the interpretation of the factors, I recommend to perform a trajectory analysis (eg Potential Source Contribution Function, or Concentration-Weighted Trajectory), especially for aged sea salt and dust. The approach proposed in the manuscript is a bit simplistic.

A2-6. *We thank the Referee for suggestion but application of PSCF/CWT needs a previous experience that we have not yet, so that we preferred not to perform an analysis before having a deep knowledge of the tool we are using. Moreover, as far as we have understood, PSCF applied on the whole*

campaign results hardly could give a realistic picture of marine air masses arriving episodically in Milan (a few events during the year originated from very different marine areas). Maybe that figure S3 (in the previous version of the paper) was a bit confusing so that we changed it with a representation where back-trajectories carrying also information on sea salt concentrations are given focusing on the episode discussed in the text.

Moreover, in many source apportionment studies factor interpretation based on chemical tracers, diagnostic ratios, seasonal contributions, etc. is often considered appropriate; in addition, in this study for a couple of factors optical variables and/or additional information not included in the model (e.g. discussion with Cl in the fine and coarse fraction for aged sea salt) strengthen the factor assignment.

Specific comments:

- p12 l325 : why road dust does thus not appear in the traffic factor ?

As reported at line 407, the road dust contribution appears to be mixed in the resuspended dust source. At lines 423-425 we added a sentence to underline this information “The lack of relevant crustal elements such as Ca and Al in the chemical profile, suggested a negligible impact of road dust in this factor. As reported above, at our sampling site the road dust contribution was very likely mixed to resuspended dust and further separation of these contributions was not possible.”

- p16 l386 : in this paragraph, I would also mention PMF studies including "Delta-C" (Wang et al., 2012), as written in the introduction.

We added the following sentence (lines 514-516): “It has to be mentioned that optical models are typically based on a two-source hypothesis (i.e. biomass burning and fossil fuel emissions); an exception reported in previous works (Wang et al., 2011) relies on the use of Delta-C used as an input variable together with chemical aerosol components in source apportionment models and proved to be very effective in separating traffic (especially diesel) emissions from wood combustion emissions”.

RESPONSE TO REVIEWER 3

R3-1. The article describes a new method to determine source-dependent absorption parameters using a receptor model based on multiple time resolution data (Crespi et al., 2016). Determination of source-dependent Angstrom exponents using C14 technique (Zotter et al., 2017) is time consuming and expensive. There is a need for alternative methods, such as the one proposed by Crespi et al. (2016).

A3-1. *As already mentioned in the response A1-1 to Referee 1, it is worth noting that the approach here presented is of general interest as (1) in this work optical data were retrieved by a home-made multi-wavelength polar photometer but the methodology here presented could be applied to dataset combining aerosol chemical and optical data obtained by widespread instrumentation (e.g. Aethalometers for optical data); (2) input data to the receptor model not necessarily should comprise variables acquired with different time resolution as we did here. We added a sentence on the general character of our work in the revised version of the paper (see lines 38-40 in the abstract and 106-110 afterwards).*

R3-2. The receptor model was run using data from the offline analysis of chemical composition and the absorption coefficient of particles collected on filters. The absorption was measured using a custom polar photometer which was validated using MAAP at a single wavelength (Vecchi et al., 2014; Bernardoni et al., 2017c). Measurements at 4 different wavelengths are used to calculate the absorption Angstrom exponent. It is not clear how accurate is the value of Angstrom exponent measured by polar photometer as it has not been compared to other multi-wavelength methods, for example: photo-acoustic spectroscopy (Lack et al., 2006), extinction minus scattering, filter photometry (Moosmuller et al., 2009) or being calibrated with laboratory generated aerosol samples (carbon black, nigrosin ...) with known spectral absorption properties and size distribution.

A3-2. *At the time of the paper submission, a laboratory experiment was in progress to intercompare PP_UniMI with optical instruments other than MAAP. The laboratory experiment was carried out at the Jülich Forschungszentrum (Germany). Preliminary data are currently available but at the moment they have been only presented in a poster by Valentini et al. at the International Conference on Carbonaceous Particles in Atmosphere in Vienna (ICCPA2019, <https://iccpa2019.univie.ac.at/abstracts/>; a copy of the poster can be requested to the authors). Briefly, samples of laboratory-generated aerosol were collected on filters and measured in parallel by on-line instrumentation. Light extinction at 450 and 630 nm was obtained by two Cavity Attenuated Phase Shift CAPS PMSSA (Aerodyne Research). An integrating Nephelometer (TSI) measured total and back-scattering coefficients at 450, 550, and 700 nm. Filter samples were analysed off-line by our polar photometer PP_UniMI.*

As far as preliminary results are concerned: the absorption Ångström exponents retrieved by extinction minus scattering method compared to data obtained by PP_UniMI measurements show a very good agreement (always well within 1 standard deviation) as reported in the mentioned poster. Therefore, in the revised version of the paper (lines 176-182) a sentence was added: “Results on b_{ap} obtained by this custom photometer resulted in very good agreement against multi-angle absorption photometer (MAAP) data at 635 nm (Vecchi et al., 2014; Bernardoni et al., 2017c). More recently, in the frame of a collaboration with the Jülich Forschungszentrum (Germany), the Absorption Ångström Exponents retrieved by extinction minus scattering measurements were compared at two wavelengths (630 nm and 450 nm) with the one obtained by PP_UniMI data for laboratory-generated aerosols. The agreement with Cabot soot was in general very good as for both b_{ap} at two wavelengths and Absorption Ångström Exponent estimates, i.e. comparability within one standard deviation (data not yet published, preliminary results reported in Valentini et al., 2019).”

R3-3. The article proposes a new set of values for the source specific Angstrom exponents for biomass burning and fossil fuel combustion: 1.83 and 0.8, respectively. The biomass burning value is in

agreement with previous studies (Zotter et al., 2017), but the value for fossil is quite low. These results are not un-expected as the summer campaign resulted in the average absorption Angstrom exponent as low as 0.58 (data from Table S2) – this value lies outside the range measured in a different settings in Europe.

A3-3. *Zotter et al. (2017) in their paper concluded that “it is recommended to use the best α combination as obtained here ($\alpha_{TR} = 0.9$ and $\alpha_{WB} = 1.68$) in future studies when no or only limited additional information like ^{14}C measurements are available” but they also stated that “a possible combination of $\alpha_{FF}=0.8$ and $\alpha_{BB}=1.8$ when EC concentration from fossil fuel combustion (estimated with radiocarbon measurements) is between 40% and 85% of the total EC concentration” (in this work, the fraction of EC ascribed by the multi-time model to fossil fuel sources was 56%).*

As now reported at lines 537-545, “The α_{BB} value retrieved by the model was very similar to values reported by Zotter et al. (2017) and also comparable to 1.86 found for biomass burning by Sandradewi et al. (2008a) and 1.8 obtained by Massabò et al. (2015) who used also independent ^{14}C measurements for checking. The α_{FF} value (assumed to be equal to α_{BC} in source apportionment optical models) resulted in the range 0.8-1.1 typically reported in optical source apportionment studies (e.g. Bernardoni et al., 2017b; Zotter et al., 2017; and references therein). Indeed, the sampling site was an urban background station in Milan where aerosol aging is a relevant process and our samples hardly had been impacted by fresh traffic emissions. Considering this feature of Milan aerosol, the average α_{FF} was included in the wide range of estimates for BC coated particles reported in literature works (approx. 0.6-1.3, Liu et al., 2018) and obtained by both ambient measurement (e.g. Fisher and Smith, 2018; and references therein) and numerical simulations (e.g. Gyawali et al., 2009; Liu et al. 2018; and references therein).”

Therefore, we concluded that (see lines 589-597): “Considering that the estimates for the Absorption Ångström Exponent were here obtained as a result of a quite complex modelling approach (i.e. using multi-time resolution datasets collected on limited periods) and without any a-priori assumption, the results obtained – although obviously affected by a certain degree of uncertainty due to both experimental data and modelling process (here estimated while often not taken into consideration for fixed α values used in the literature) – were fairly comparable to literature results and gave a further tool aimed at assessing more robust source-related α values. In perspective, joining together different approaches such as the receptor modelling here proposed and e.g. ^{14}C measurements and artefact-free b_{ap} measurements will likely lead to better estimates of the Absorption Ångström Exponent; work is in progress at our laboratories to achieve this goal.”

In literature works, it is rarely taken into account that α is also very sensitive to small variations in b_{ap} values; indeed, considering α estimates based on experimental data with e.g. uncertainties of about 10% (which is a quite common estimate for uncertainty associated to absorption optical measurements) effects on the retrieved value can be relevant.

R3-4. It is also strange that there is no wavelength dependency in absorption coefficients between 532 and 780 nm for the traffic component (Figure 1). Authors should provide an extensive quality control assessment of absorption data to support their findings.

A3-4.: *The Referee is right but it must be taken into account that b_{ap} was splitted by the model into different sources with a degree of uncertainty given by the modelling approach itself. This is the first work coupling multi-time resolution and multi-variable datasets so that further applications – e.g. with larger temporal coverage and from different sites – will likely indicate us which is the parameter to be optimized in the model to retrieve the best overall result. However, as already mentioned, the estimates here reported can be surely considered not less robust than those often taken a-priori in other literature works.*

R3-6. Raw measurements (time-series, diurnal profile) should be presented and discussed before proceeding to the data evaluation using the receptor model.

A3-6.: *Following the Referee's request we added a section (Sect. 3.1 in the revised text) where a general description of the dataset is given. As for time series of raw measurements, we decided to present them only when necessary for sources interpretation (see the aged sea-salt source, Figure 2 and S3) in order to avoid redundant information.*

R3-7. The language in certain parts of the article is not clear.

A3-7. *English language and grammar was thoroughly revised*

Here are some specific remarks:

- the parameter describing the spectral dependence of the absorption coefficient is usually named Absorption Angstrom Exponent (similar to Scattering Angstrom Exponent).

Correction done

- the term Multi-time source apportionment study is not clear. The term Multi-time resolution source apportionment is proposed.

Following literature papers dealing with this kind of analysis we omitted the term "resolution"; however, for clarity it has been now added.

- Line 20: MAC should be defined as Mass Absorption Cross-section instead of Mass Absorption Coefficient

Correction done.

I recommend performing another review after extensive revision of the manuscript. Concerning the scope of the journal, the article might be better suited for the publication in AMT.

This kind switch can be done at the initial submission stage and not after the long discussion phase on ACPD. We would like also to remark that both Referees at the initial stage evaluated the paper suitable for publication on ACPD.

References

- Bernardoni V., Valli G. and Vecchi R.: Set-up of a multi-wavelength polar photometer for the off-line measurement of light absorption properties of atmospheric aerosol collected with high-temporal resolution, *J. Aerosol. Sci.*, 107, 84-93, 2017
- Fischer D.A. and Smith G.D.: A portable, four wavelength, single-cell photoacoustic spectrometer for ambient aerosol absorption, *Aerosol Sci. Tech.*, 52, 393-406, 2018
- Gyawali M., Arnott W.P., Lewis K. and Moosmüller H.: In situ aerosol optics in Reno, NV, USA during and after the summer 2008 California wildfires and the influence of absorbing and non-absorbing organic coatings on spectral light absorption, *Atmos.Chem.Phys*, 9, 2009
- Liu C., Chung C.E., Yin Y. and Schnaiter M.: The absorption Ångström exponent of black carbon: from numerical aspects. *Atmos. Chem. Phys.*, 18, 6259-6273, 2018
- Valentini et al. (2019); Multi-Wavelength Measurement of Aerosol Optical Properties: Laboratory Intercomparison of In-Situ and Filter-Based Techniques; 12th International Conference on Carbonaceous Particles in the Atmosphere (ICCPA) 2019 <https://iccpa2019.univie.ac.at/abstracts/>
- Vecchi R., Bernardoni V., Paganelli C. and Valli G.: A filter-based light absorption measurement with polar photometer: effects of sampling artefacts from organic carbon, *J. Aerosol. Sci.*, 70, 15-25, 2014
- Zotter P., Herich H., Gysel M., El-Haddad I., Zhang Y., Mocnik G., Hüglin C., Baltensperger U., Szidat S. and Prévôt A.S.H.: Evaluation of the absorption Ångström exponents for traffic and wood burning in the Aethalometer-based source apportionment using radiocarbon measurements of ambient aerosol, *Atmos. Chem. Phys.*, 17, 4229-4249, 2017

1 Exploiting multi-wavelength aerosol absorption coefficients in a 2 multi-time resolution source apportionment study to retrieve 3 source-dependent absorption parameters

4 Alice C. Forello¹, Vera Bernardoni¹, Giulia Calzolai², Franco Lucarelli², Dario Massabò³, Silvia
5 Nava², Rosaria E. Pileci^{1,a}, Paolo Prati³, Sara Valentini¹, Gianluigi Valli¹, Roberta Vecchi^{1,*}

6 ¹Department of Physics, Università degli Studi di Milano and National Institute of Nuclear Physics INFN-Milan, via
7 Celoria 16, Milan, 20133, Italy

8 ²Department of Physics and Astronomy, Università di Firenze and National Institute of Nuclear Physics INFN-Florence,
9 via G. Sansone 1, Sesto Fiorentino, 50019, Italy

10 ³Department of Physics, Università degli Studi di Genova and National Institute of Nuclear Physics INFN- Genoa, via
11 Dodecaneso 33, Genoa, 16146, Italy

12 ^anow at: Laboratory of Atmospheric Chemistry (LAC), Paul Scherrer Institut (PSI), Forschungsstrasse 111, Villigen,
13 5232, Switzerland

14

15 **Correspondence to:* Roberta Vecchi (roberta.vecchi@unimi.it)

16

17 **Abstract.** In this paper, a new methodology coupling aerosol optical and chemical parameters in the same source
18 apportionment study is reported. In addition to results on sources assessment, ~~This~~ approach gives ~~additional~~ relevant
19 information such as estimates for the atmospheric ~~Ångström~~-Absorption Ångström Exponent (α) of the sources and ~~Mass~~
20 ~~Absorption Coefficient~~ Mass Absorption Cross section (MAC) for fossil fuel emissions at different wavelengths.

21 A ~~multi-time~~ multi-time resolution source apportionment study using Multilinear Engine ME-2 was performed on a PM10
22 dataset with different time resolution (24 hours, 12 hours, and 1 hour) collected during two different seasons in Milan
23 (Italy) in 2016. Samples were optically analysed to retrieve the aerosol absorption coefficient b_{ap} (in Mm^{-1}) at four
24 wavelengths ($\lambda=405$ nm, 532 nm, 635 nm and 780 nm) and chemically characterised for elements, ions, levoglucosan,
25 and carbonaceous components. Time-resolved chemically speciated data were ~~coupled-joined to with~~ b_{ap} multi-wavelength
26 measurements and ~~introduce~~ used as input data in the ~~multi-time~~ multi-time resolution receptor model; this approach was
27 proven to strengthen the identification of sources being particularly useful when important chemical markers (e.g.
28 levoglucosan, elemental carbon, ...) are not available. The final solution consisted in 8 factors (nitrate, sulphate,

29 resuspended dust, biomass burning, construction works, traffic, industry, aged sea salt); the implemented constraints led
30 to a better physical description of factors and the bootstrap analysis supported the goodness of the solution. As for b_{ap}
31 apportionment, consistently to what expected, the two factors assigned to biomass burning and traffic were the main
32 contributors to aerosol absorption in atmosphere. A relevant feature of the approach proposed in this work is the possibility
33 of retrieving many other information about optical parameters; for example, opposite to the more traditional approach
34 used by optical source apportionment models, here we obtained the atmospheric Absorption Ångström Exponent (α) of
35 the sources (α biomass burning = 1.83 and α fossil fuels = 0.80), without any a priori assumption. In addition, an estimate
36 for the Mass Absorption Cross section (MAC) for fossil fuel emissions at four wavelengths was obtained and found to be
37 consistent with literature ranges.

38 It is worth noting that the approach here presented can be also applied using widespread receptor models (e.g. EPA PMF
39 instead of multi-time resolution ME-2) if the dataset comprises variables with the same time resolution as well as optical
40 data retrieved by commercial instrumentation (e.g. an Aethalometer instead of home-made instrumentation).

41

42 1. Introduction

43 Atmospheric aerosol impacts both on local and global scale causing adverse health effects (Pope and Dockery, 2006),
44 decreasing visibility (Watson, 2002) and influencing the climate (IPCC, 2013). To face these issues an accurate
45 knowledge of ~~the~~ aerosol emission sources is mandatory.

46 At the state of the art, multivariate receptor models are considered a robust approach (Belis et al., 2015) to ~~carry out~~
47 ~~perform~~ source apportionment studies ~~of atmospheric aerosol~~ and the Positive Matrix Factorization (PMF) (Paatero and
48 Tapper, 1994) has become one of the most widely used receptor models (Hopke, 2016) in the aerosol community. In the
49 late 1990s the Multilinear Engine (ME-2) was ~~implemented, developed and proved to be~~ a very flexible algorithm to
50 solve multilinear and quasi-multilinear problems (Paatero, 1999). ~~This algorithm introduced the possibility to write scripts~~
51 ~~and implement~~ The scripting feature of this algorithm allows the implementation of advanced receptor modelling
52 approaches; one example is the ~~multi-time~~ multi-time resolution model, developed for the first time by Zhou et al. (2004),
53 which uses each experimental data in its original time schedule as model input. Source apportionment studies carried out
54 by multi-time resolution model are still scarce in the literature (Zhou et al., 2004; Ogulei et al., 2005; Kuo et al., 2014;
55 Liao et al., 2015; Crespi et al., 2016; Sofowote et al., 2018) although t ~~This approach methodology~~ is very useful in
56 measurement campaigns when instrumentation with different time resolution (minutes, hours or days) is available ~~as~~
57 ~~indeed, with the multi-time approach,~~ high time resolution data can be exploited without averaging them over the longest
58 sampling interval. ~~Nevertheless, source apportionment studies carried out by multi-time model are still scarce in the~~

59 ~~literature (Zhou et al., 2004; Ogulei et al., 2005; Kuo et al., 2014; Liao et al., 2015; Crespi et al., 2016; Sofowote et al.,~~
60 ~~2018).~~

61 It is noteworthy that (The combination of time-resolved chemically speciated data with the information obtained from
62 instrumentation measuring aerosol optical properties at different wavelengths (e.g. the absorption coefficient b_{ap}) is
63 suggested as one of the future investigations of receptor modelling (Hopke, 2016); however, to the best of our knowledge,
64 very few attempts in this direction have been done (~~recently~~ e.g. Peré-Trepat et al., 2007; Xie et al., 2019). Wang et al.
65 (2011, 2012) introduced in a source apportionment study the Delta-C (Delta-C = BC@370 nm – BC@880 nm from
66 ~~aethalometer~~ Aethalometer measurements) as an input variable ~~in a source apportionment study~~ and found that Delta-C
67 was very useful in separating traffic from ~~wood~~ biomass burning source contributions.

68 The wavelength dependence of the aerosol absorption coefficient (b_{ap}) can be empirically considered proportional to $\lambda^{-\alpha}$,
69 where α is the ~~Ångström~~ Absorption Ångström Exponent; α depends on particles composition and size, and it is a useful
70 parameter to gain information about particles type in atmosphere (see e.g. Yang et al., 2009). Among PM components,
71 black carbon (BC) is the main responsible for light absorption in atmosphere; in fact, it is considered the main PM
72 contributor to global warming and the second most important anthropogenic contributor after CO₂ (Bond et al., 2013).
73 Black carbon refers to a fraction of the carbonaceous aerosol that shares peculiar features about microstructure,
74 morphology, thermal stability, solubility, and light absorption (Petzold et al., 2013); in particular, it is characterised by a
75 wavelength-independent imaginary part of the refractive index over visible and near-visible regions. In the last decade,
76 experimental studies evidenced also the role of another absorbing component i.e. brown carbon (BrC), referred to as light-
77 absorbing organic matter of various origins with increasing absorption towards lower wavelengths, especially in the UV
78 region (Andreae and Gelencsér, 2006). BrC is an aerosol component that also affects the elemental vs. organic carbon
79 correct separation when using thermal-optical methods as recently outlined by Massabò et al. (2016).

80 Source apportionment optical models based only on multi-wavelength measurements of b_{ap} are available in the literature,
81 i.e. the widespread Aethalometer model (Sandradewi et al., 2008a) and the more recent Multi-Wavelength Absorption
82 Analyzer (MWAA) model (Massabò et al., 2015; Bernardoni et al., 2017b). Briefly, these models allow to estimate the
83 contribution of sources to aerosol absorption in atmosphere exploiting their different dependence on λ (different α). As a
84 step forward, MWAA provides the b_{ap} apportionment in relation to both the sources and the components (i.e. BC and
85 BrC) and gives also an estimate for α of BrC. Source apportionment optical models usually assume two contributors to
86 b_{ap} , namely fossil fuels combustion and ~~wood~~ biomass burning (only few exceptions are present in the literature, e.g.
87 Fialho et al., 2005). In most cases this assumption is well founded, except in presence of episodic events that give a not
88 negligible contribution to aerosol absorption in atmosphere, such as the transport of mineral dust from the Saharan desert
89 (Fuzzi et al., 2015). Moreover, the above-mentioned models need a priori assumption about α values of the sources; this

90 is the most critical step, since α depends on the kind of fuel, burning conditions and aging processes in the atmosphere
91 and wide ranges for α are reported in literature (e.g. Sandradewi et al., 2008a). Without accurate determination of source-
92 specific atmospheric α (for example exploiting the information derived from source apportionment using ^{14}C
93 measurements), the applicability of models based on optical ~~determination measurements~~ is questionable (Bernardoni et
94 al., 2017b; Massabò et al., 2015; Zotter et al., 2017). Moreover, the generally accepted assumption of $\alpha=1$ for fossil fuels
95 and BC, that is derived from the theory of absorption of spherical particles in the Rayleigh regime (Seinfeld and Pandis,
96 2006), might not always be valid in atmosphere due to aerosol aging processes (Liu et al., 2018).

97 ~~In this work, i~~In the frame of a source apportionment study based on ~~multi-time~~multi-time resolution receptor modelling,
98 ~~in this work~~ optical and chemical data~~sets~~ were ~~joined~~coupled to explore the possibility of retrieving a multi- λ
99 apportionment of b_{ap} with no need of a-priori assumptions on the contributing sources. Opposite, with this approach
100 source-dependent α values ~~can be were~~ provided as output. Moreover, the multi- λ apportionment of b_{ap} in each source
101 allowed to estimate MAC values at different wavelengths, exploiting the well-known relation $\text{EBC} = b_{\text{ap}}(\lambda) / \text{MAC}(\lambda)$ (Bond
102 and Bergstrom, 2006) and considering the apportioned concentrations of elemental carbon (EC) as a proxy for BC. ~~It is~~
103 ~~noteworthy that~~ ~~t~~The evaluation of atmospheric MAC values is also not trivial due to the possible presence of absorbing
104 components different from BC (e.g. contribution from BrC, especially at lower wavelengths).

105 The original approach proposed in this work shows that coupling the chemical and optical information in a receptor
106 modelling process is particularly advantageous because: (1) strengthens the source identification, that is particularly
107 useful when relevant chemical tracers (e.g. levoglucosan, EC, ...) are not available; (2) gives estimates for source-specific
108 atmospheric Absorption Ångström Exponent (α) which are typically assumed a-priori in optical apportionment models;
109 (3) assesses MAC values at different wavelengths for specific sources.

110 It is also worth noting that the approach here presented is of general interest as (1) in this work optical data were retrieved
111 by a home-made multi-wavelength polar photometer but~~photometer but~~ the same methodology could be applied to
112 datasets combining aerosol chemical and optical data obtained by widespread instrumentation (e.g. Aethalometers for
113 optical data); (2) input data to the receptor model not necessarily should comprise variables acquired with different time
114 resolution as we did here.

115

116 2. Material and methods

117 2.1 Site description and aerosol sampling

118 Two measurement campaigns were performed during summertime (June-July) and wintertime (November-December)
119 2016 in Milan (Italy). Milan is the largest city (more than 1 million inhabitants, doubled by commuters everyday) of the

120 Po Valley, a very well-known hot-spot pollution area in Europe due to both large emissions from a variety of sources (i.e.
121 traffic, industry, domestic heating, energy production plants, and agriculture) and low atmospheric dispersion conditions
122 (e.g. Vecchi et al., 2007 and 2019; Perrone et al., 2012; Bigi and Ghermandi, 2014; Perrino et al., 2014).

123 The sampling site is representative of the urban background and it is situated at about 10 meters above the ground, on the
124 roof of the Physics Department of the University of Milan, less than 4 km far from the city centre (Vecchi et al., 2009).

125 It is important to note that during the sampling campaigns, a large building site was in activity next to the monitoring
126 station.

127 Aerosol sampling was carried out using instrumentation with different time-resolution. Low time resolution PM10 data,
128 with a sampling duration of 24 and 12 hours during summertime (20 June-22 July 2016) and wintertime (21 November-
129 22 December 2016), respectively, were collected in parallel on PTFE (Whatman, 47 mm diameter) and pre-fired (700 °C,
130 1 hour) quartz-fibre (Pall, 2500QAO-UP, 47 mm diameter) filters. Low volume samplers with EPA PM10 inlet operating
131 at 1 m³ h⁻¹ were used. High time resolution data were collected during shorter periods (11 July-18 July and 21 November-
132 28 November 2016) by a streaker sampler (D'Alessandro et al., 2003). Shortly, the streaker sampler collects the fine and
133 coarse PM fractions (particles with aerodynamic diameter $d_{ae} < 2.5 \mu\text{m}$, and $2.5 < d_{ae} < 10 \mu\text{m}$, respectively) with hourly
134 resolution. Particles with $d_{ae} > 10 \mu\text{m}$ impact on the first stage and are discarded; the coarse fraction deposits on the second
135 stage, consisting of a Kapton foil; finally, the fine fraction is collected on a polycarbonate filter. The two collecting
136 supports are kept in rotation with an angular speed of about 1.8° h⁻¹ to produce a circular continuous deposit on both
137 stages.

138 Meteorological data were available at a monitoring station belonging to the regional environmental agency (ARPA
139 Lombardia) which is less than 1 km far away.

140

141 2.2 PM mass concentration and chemical characterisation

142 ~~In this Section, we resume the chemical analyses performed on samples are summarised. As mEach measured~~
143 ~~concentration in each sample is was characterised by its own uncertainty, only ; here we report ranges for experimental~~
144 ~~uncertainties and Minimum Detection Limits (MDLs) for each every set of variables are reported analysis. These~~
145 ~~values were used as starting points to estimate the uncertainties introduced in the model (see also Sect. 2.5).~~

146 PM10 mass concentration was determined on PTFE filters by gravimetric technique. Weighing was performed by an
147 analytical balance (Mettler, model UMT5, 1 µg sensitivity) after a 24 hours conditioning period in an air-controlled room
148 as for temperature ($20 \pm 1 \text{ }^\circ\text{C}$) and relative humidity ($50 \pm 3 \%$) (Vecchi et al., 2004).

149 These filters were then analysed by Energy Dispersive X-Ray Fluorescence (ED-XRF) analysis to obtain the elemental
150 composition (details on the procedure can be found in Vecchi et al., 2004). For most elements and samples, concentrations

151 were characterised by relative uncertainties in the range 7-20 % (higher uncertainties for elements with concentrations
152 next to MDLs) and ~~Minimum-minimum Detection-detection Limits-limits (MDL)~~ of 0.9-30 ng m⁻³ with the above
153 mentioned sampling conditions. ~~Quartz fibre filters were punched and analysed to detect levoglucosan, sulphate, nitrate,
154 and carbonaceous components.~~

155 For each quartz-fibre filter, one punch (1.5 cm²) was extracted by sonication (1 h) using 5 ml ultrapure Milli-Q water;
156 this extract was analysed to measure both levoglucosan and inorganic anions concentrations. Levoglucosan concentration
157 was determined by High-Performance Anion Exchange Chromatography coupled with Pulsed Amperometric Detection
158 (HPAEC-PAD) (Piazzalunga et al., 2010) only in winter samples. Indeed, as already pointed out by other studies at the
159 same sampling site (Bernardoni et al., 2011) and as routinely measured at monitoring stations in Milan by the Regional
160 Environmental Agency (private communication), levoglucosan concentrations during summertime are lower than the
161 MDL of the technique (about 6 ng m⁻³), due to both lower emissions (no influence of residential heating and negligible
162 impact from other sources) and higher OH levels in the atmosphere depleting molecular markers concentrations (Robinson
163 et al., 2006; Hennigan et al., 2010). Uncertainties on levoglucosan concentration were about 11 % . The measurement
164 of main water-soluble inorganic anions (SO₄²⁻ and NO₃⁻) was performed by Ion Chromatography (IC); ~~these data had with~~
165 MDL of 25 and 50 ng m⁻³ with summertime and wintertime sampling conditions, respectively, and uncertainties of about
166 10 % . Unfortunately, due to technical problems no data on ammonium were available. Details on the analytical
167 procedure for IC analysis are reported in Piazzalunga et al. (2013).

168 Another punch (1.0 cm²) of each quartz-fibre filter was analysed by Thermal Optical Transmittance analysis (TOT, Sunset
169 Inc., NIOSH-870 protocol) (Piazzalunga et al., 2011) in order to assess organic and elemental carbon (OC and EC)
170 concentrations. MDL was 75 and 150 ng m⁻³ with summertime and wintertime sampling conditions, respectively, and
171 uncertainties were ~~about in the range~~ 10-15 % .

172 ~~High time resolution samples were analysed to obtain the~~Hourly elemental composition was assessed by Particle Induced
173 X-ray Emission (PIXE) technique, using a properly collimated proton beam and scanning the deposits in steps
174 corresponding to 1-hour aerosol deposit (details in Calzolari et al., 2015). In this work, fine and coarse elemental
175 concentrations determined by PIXE analysis were added up to obtain PM10 concentrations with hourly resolution as low
176 time resolution PM10 samples were also available. PM10 hourly concentrations of most elements and samples were
177 characterised by relative uncertainties in the range 10-30% (higher uncertainties for elements near MDL) and MDLs
178 ranged from a minimum of 0.1 to a maximum of 15 ng m⁻³ (higher MDLs typically detected for Z<20 elements).

179

180 2.3 Aerosol light-absorption coefficient measurements

181 The aerosol absorption coefficient (b_{ap}) at the 4 wavelengths $\lambda = 405, 532, 635$ and 780 nm was measured on both low
182 and high time resolution samples with the home-made polar photometer PP_UniMI (Vecchi et al., 2014; Bernardoni et
183 al., 2017c). Results on b_{ap} obtained by this custom photometer resulted in very good agreement against multi-angle
184 absorption photometer (MAAP) data at 635 nm (Vecchi et al., 2014; Bernardoni et al., 2017c). More recently, in the frame
185 of a collaboration with the Jülich Forschungszentrum (Germany), the Absorption Ångström Exponents retrieved by
186 extinction minus scattering measurements were compared at two wavelengths (630 nm and 450 nm) with the one obtained
187 by PP_UniMI data for laboratory-generated aerosols. The agreement with Cabot soot was in general very good as for
188 both b_{ap} at two wavelengths and Absorption Ångström Exponent estimates, i.e. comparability within one standard
189 deviation (data not yet published, preliminary results reported in Valentini et al., 2019).

190 Low time resolution optical measurements taken into account were those performed on PTFE filters since their physical
191 characteristics can be considered more similar to polycarbonate filters used by the streaker sampler. Moreover, previous
192 works reported a bias on b_{ap} measured by instrumentation using fibre filters (e.g. Cappa et al., 2008; Lack et al., 2008;
193 Davies et al., 2019; and references therein); Vecchi et al. (2014) quantified in about 40% % the effect caused in b_{ap} values
194 (assessed at 635 nm) by sampling artefacts due to organics in aerosol samples collected in Milan when comparing aerosol
195 samples collected in parallel quartz-fibre and PTFE filters.

196 ~~Indeed, Vecchi et al. (2014) reported that aerosol absorption measurements on samples collected in parallel on quartz-~~
197 ~~fibre and PTFE filters showed significant differences, which were mainly ascribed to sampling artefacts due to organics~~
198 ~~affecting quartz-fibre filters.~~ For high time resolution samples, b_{ap} was measured only in the fine fraction collected on
199 polycarbonate filters, since absorption from the Kapton foil on which the coarse fraction was collected did not allow b_{ap}
200 assessment. Anyway, b_{ap} values in PM2.5 and PM10 were expected to be fairly comparable, as most of the contribution
201 to aerosol absorption in atmosphere is typically given by particles in the fine fraction at heavily polluted urban sites like
202 Milan. To verify this assumption, high time resolution b_{ap} data in PM2.5 were averaged on the time scale of low time
203 resolution b_{ap} in PM10 for comparison. They turned out to be in good agreement, between 11 % % and 13 % % depending
204 on the λ , except for b_{ap} at $\lambda=405$ nm that showed a higher difference (27 % %) but with most data (83 % %) within
205 experimental uncertainties. To take into account for this difference, b_{ap} data at $\lambda=405$ nm were homogenised before their
206 insertion into the model, following the criterion used for chemical species (for further detail about homogenisation
207 procedure, see Sect. 2.4 and Sect. 2.5).

208 Uncertainties on b_{ap} were estimated as 15 %-% % and MDL was in the range 1-10 Mm⁻¹ depending on sampling duration
209 and wavelength as already reported in our previous works (Vecchi et al., 2014; Bernardoni et al., 2017c). Experimental
210 uncertainties and MDL of optical absorption data were used as a starting point to estimate the uncertainties introduced in
211 the model. Pre-treatment procedure for these data was the same of chemical ones variables (see also Sect. 2.5). Optical

212 system stability was checked during the measurement session, evaluating the reproducibility ~~of the measure of of the~~
213 ~~measurement on~~ a blank test filter. Laser stability was also checked at least twice a day and the recorded intensities were
214 used to normalise blank and sampled filters analysis.

215

216 2.4 Model description

217 Multivariate receptor models (Henry, 1997) ~~represent one of are among~~ the most widespread and robust approaches used
218 to carry out source apportionment studies for atmospheric aerosol (Belis et al., 2014 and 2015). In particular, the Positive
219 Matrix Factorization (Paatero and Tapper, 1994; Paatero, 1997) ~~has had~~ been extensively used in the literature and,
220 afterwards, the Multilinear Engine ME2 (Paatero, 1999 and 2000) introduced the possibility of solving all kinds of
221 multilinear and quasi-multilinear problems. The fundamental principle ~~of these modelling approaches~~ is the mass
222 conservation between the emission source and the receptor site ~~using focusing on the the information carried by~~ aerosol
223 ~~properties-chemical composition assessed on a number of samples collected~~ at the receptor site ~~(i.e. measuring a large~~
224 ~~number of chemical constituents in different samples)~~, a mass balance analysis can be performed to identify the factors
225 influencing aerosol mass concentrations (Hopke, 2016). Factors can be subsequently interpreted as the main sources
226 impacting the site, exploiting ~~the characterisation of knowledge about~~ the most relevant sources in the investigated area
227 ~~and/or~~ the adoption of fingerprints available from previous literature works (Belis et al., 2014). Referring to the input data
228 as matrix X (matrix elements x_{ij}), the chemical profile of the factors as matrix F (matrix elements f_{kj}), and the time
229 contribution of the factors as matrix G (matrix elements g_{ik}), the main equation of a bilinear problem can be written as
230 follows:

$$231 \quad x_{ij} = \sum_{k=1}^P g_{ik} f_{kj} + e_{ij} \quad (1)$$

232 where the indices i, j, and k indicate the sample, the species, and the factor, respectively; P is the number of factors and
233 the matrix E (matrix elements e_{ij}) is composed by the residuals, i.e. the difference between measured and modelled values.
234 In this way, a system of NxM equations is established, where N is the number of samples and M is the number of species.
235 The solution of the problem is computed minimising the object function Q defined as:

$$236 \quad Q = \sum_{i=1}^N \sum_{j=1}^M \left(\frac{e_{ij}}{\sigma_{ij}} \right)^2 \quad (2)$$

237 where σ_{ij} are the uncertainties related to the input data.

238 The ~~multi-time~~ multi-time resolution receptor model was developed in order to use each data value in its original time
239 schedule, without averaging the high time resolution data or interpolating the low time resolution data (Zhou et al., 2004;
240 Ogulei et al., 2005). The main Eq. (1) is consequently modified as below:

241
$$x_{sj} = \frac{1}{t_{s2}-t_{s1}+1} \sum_{k=1}^P f_{kj} \sum_{i=t_{s1}}^{t_{s2}} g_{ik} \eta_{jm} + e_{sj} \quad (3)$$

242 where the indices s, j, and k indicate the sample, the species and the factor respectively; P is the number of factors; t_{s1} and
243 t_{s2} are the starting and ending time for the s-th sample in time units (i.e. the shortest sampling interval, that is 1 hour for
244 the dataset ~~of this work~~ [used here](#)) and i represents one of the time units of the s-th sample. η_{jm} are adjustment factors for
245 chemical species replicated with different time resolution and measured with different analytical methods (represented
246 by the subscript m).

247 If η is close to unity, species concentration measured by different analytical approaches can be considered in good
248 agreement; non-replicated species have adjustment factors set to unity by default. In this work, the adjustment factors
249 were always set to unity in the model; to take into account the use of different aerosol samplers (i.e. low volume sampler
250 with EPA inlet and streaker sampler) and different analytical techniques to obtain the elemental composition (i.e. ED-
251 XRF and PIXE), concentrations of replicated species with different time resolution were homogenised before inserting
252 them into the input matrix X, as will be explained in Sect. 2.5. Applying this data treatment procedure, it is possible to
253 avoid ~~the to~~ check ~~of the consistency, from the experimental point of view, of~~ the η values calculated by the model ~~are~~
254 [consistent with differences in experimental data characterised by high and low time resolution](#). Otherwise, this step should
255 always be performed after running the model.

256 In the ~~multi-time~~ [multi-time resolution](#) model a regularisation equation is introduced, since some sources could contain
257 few or no species measured with high time resolution:

258
$$g_{(i+1)k} - g_{ik} = 0 + \varepsilon_i \quad (4)$$

259 where ε_i represent the residuals.

260 As already pointed out ~~in a previous work~~ (by Ogulei et al. (=2005), a weighing parameter for low resolution species (~~24~~
261 ~~or 12 hours in this work~~) might be necessary; in this study, it was implemented in the equations and set at 0.5 for strong
262 species (not applied to weaker species as Na, Mg, and Cr, see Sect. 2.5) [in 24-h or 12-h samples](#).

263 Equations (3) and (4) ~~were~~ [are](#) solved using the Multilinear Engine (ME) program (Paatero, 1999). In Eq. (2), the object
264 function Q takes into account residuals from the main Eq. (3) and from the auxiliary equations (regularisation Eq. (4),
265 normalisation equation, pulling equations, and constraints).

266 In this work, the ~~multi-time~~ [multi-time resolution](#) model implemented by Crespi et al. (2016) ~~is~~ [was](#) used; ~~therefore,~~ ~~Using~~
267 ~~this model implementation,~~ constraints ~~can be~~ [were](#) inserted in the model and the bootstrap analysis ~~is~~ [was](#) also performed
268 to evaluate the robustness of the final solution.

269

270 *2.5 Input data*

271 As already mentioned in Sect. 2.4, instead of using adjustment factors in the model (all set equal to one), concentrations
272 of replicated species with different time resolution were pre-homogenised and then inserted into the input matrix X.
273 Concentration data with longer sampling interval (24 and 12 hours in this work) were considered as benchmark, since
274 analytical techniques usually show a better accuracy on concentration values far from MDL (i.e. samples collected on
275 longer time intervals) (Zhou et al., 2004; Ogulei et al., 2005).

276 Variables were then classified as weak and strong ~~based on~~according to the ~~signal-signal-to-to~~ noise ratio (S/N) criterion
277 (Paatero, 2015). For hourly data only strong variables ($S/N \geq 1.2$) were considered; for low time resolution data also
278 weaker variables as Na, Mg and Cr (with S/N equal to about 0.8), that resulted strong variables in hourly samples, were
279 also ~~inserted~~included although under-weighted (i.e. ~~associated with~~ uncertainties comparable to concentration values) in
280 order to avoid the exclusion of too many data. Indeed, excluding these low time resolution variables from the analysis
281 gave rise to artificial high values in the ~~source~~ time contribution matrix for ~~these~~ sources traced by these species (in this
282 case it was particularly important for aged sea salt traced by Na and Mg, see Sect. 3.2+); this oddity was already reported
283 by Zhou et al. (2004).

284 Each~~every~~ measured variable in each sample is characterised by its own uncertainty: range of experimental uncertainties
285 and MDL are reported in Sect. 2.2 and 2.3 for chemical and optical analyses, respectively. Variables with more than 20
286 ~~%~~ % of the concentration data below MDL values were omitted from the analysis (Ogulei et al., 2005). The procedure
287 described in Polissar et al. (1998) was followed to treat uncertainties and below MDL data, starting from experimental
288 uncertainties and MDLs. In general, missing concentration values were estimated by linear interpolation of the measured
289 data and their uncertainties were assumed as three times this estimated value (Zhou et al., 2004; Ogulei et al., 2005). As
290 for summertime levoglucosan data (not available), the approach was to include them as below MDL data and not as
291 missing data following Zhou et al. (2004), who underlined that the ~~multi-time~~multi-time resolution model is more
292 sensitive to missing values than the original PMF model. In order to avoid double counting, in this study S was chosen as
293 input variable instead of SO_4^{2-} as it was determined on both low time- and high time-resolution samples (by XRF and
294 PIXE analysis, respectively, see Calzolari et al., 2008). However, elemental SO_4^{2-} and S concentrations showed a high
295 correlation (correlation coefficient $R=0.98$) and the Deming regression gave a slope of 2.69 ± 0.13 (sulphate vs. sulphur)
296 with an intercept of -198 ± 82 , i.e. compatible with zero within 3 standard deviations. The slight difference (of the order
297 of ~~10%~~ %) between the estimated slope and the SO_4^{2-} -to-S stoichiometric coefficient (i.e. 3) can be ascribed to either a
298 small fraction of insoluble sulphate or to the use of different analytical techniques.

299 PM10 mass concentrations were included in the model with uncertainties set at four times their values (Kim et al., 2003).
300 In the end, 22 low time resolution variables (PM10 mass, Na, Mg, Al, Si, S, K, Ca, Cr, Mn, Fe, Cu, Zn, Pb, EC, OC,

301 levoglucosan, NO₃⁻, b_{ap} 405nm, b_{ap} 532nm, b_{ap} 635nm, b_{ap} 780nm) and 17 hourly variables (Na, Mg, Al, Si, S, K, Ca, Cr,
302 Mn, Fe, Cu, Zn, Pb, b_{ap} 405nm, b_{ap} 532nm, b_{ap} 635nm, b_{ap} 780nm) were considered.

303 ~~Finally,~~ The input matrix **X** consisted in 386 samples and the total number of time units was 1117. The analysis was
304 performed in the robust mode; lower limit for G contribution was set to -0.2 (Brown et al., 2015) and the error model
305 em=-14 was used for the main equation with C₁= input error, C₂= 0.0 and C₃=0.1 (Paatero, 2012) [for both chemical and](#)
306 [optical absorption data](#).

307 [Sensitivity tests on the uncertainty of absorption data were performed starting from a minimum uncertainty of 10% %.](#)
308 [Lower uncertainties were considered not physically meaningful from an experimental point of view. ME-2 analyses](#)
309 [performed with 10% % uncertainty on absorption data gave very similar results to the base case solution presented in the](#)
310 [Supplement \(Figure S1 and Table S+3\), with no differences in mass apportionment and a maximum variation in the](#)
311 [concentrations of chemical and optical profiles \(matrix F\) of 7% % when considering significant variables in each profile](#)
312 [\(i.e. EVF higher or near 0.30\). Opposite, considering an uncertainty of 20% % on absorption data, the solution](#)
313 [significantly differed from the base case one presented in the Supplement and showed less physical meaning. Indeed, the](#)
314 [factors assigned to resuspended dust and construction works got mixed, and a new unique factor \(traced almost](#)
315 [exclusively by Pb\) appeared, with mass contribution equal to zero. Thus, the estimated relative uncertainty of 15% % was](#)
316 [here considered appropriate for optical variables \(but for b_{ap} at 405 nm, as already mentioned\).](#)

317 [It is also noteworthy that ME-2/PMF analysis is not a-priori harmed by the use of joint matrices containing different units](#)
318 [\(see e.g. Paatero, 2018\). Indeed, if different units are present in different columns of matrix X, the output data in factor](#)
319 [matrix G are pure numbers and elements in a column of factor matrix F carry the same dimension and unit as the original](#)
320 [data in matrix X. In addition, as we did in this work, the average total contribution to the mass of a specific source due to](#)
321 [species in a certain factor in matrix F must be retrieved a-posteriori summing up only mass contributions by chemical](#)
322 [components \(i.e. excluding optical components in matrix F\).](#)

323 To the authors' knowledge, this is the first time that [the absorption coefficients b_{ap} at different wavelengths](#) ~~has been~~
324 introduced in the ~~multi-time~~ [multi-time resolution](#) model and used to more robustly identify the sources; moreover, the
325 optical information ~~has been~~ [was](#) also exploited to retrieve additional information such as the Absorption Ångström
326 Exponent (α) of the sources and MAC values in an original way.

327

328 **3. Results and discussion**

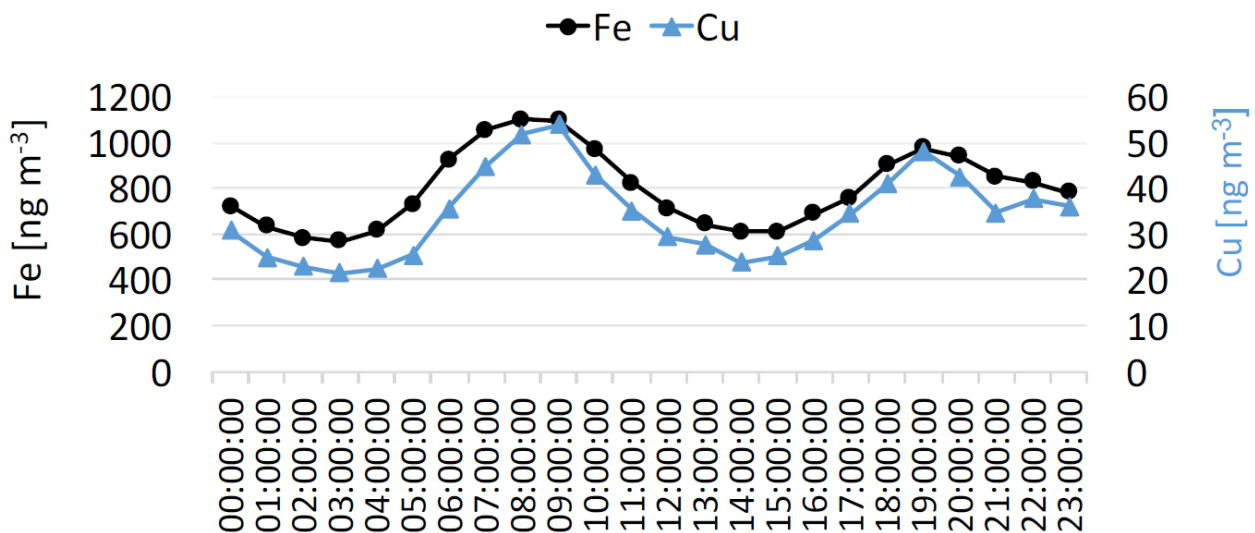
329 [3.1 Concentration values](#)

330 [In Table S1 \(Supplement\) basic statistics on mass and chemical species concentrations at different time resolution are](#)
331 [given.](#)

332 Most variables showed higher mean and median concentrations during the winter campaign, when atmospheric stability
 333 conditions influenced the monitoring site; exceptions were Al, Si and Ca which had lower median concentrations (as
 334 detected in low time resolution samples). This was not unexpected as they are typical tracers of soil dust resuspension
 335 (Viana et al., 2008) that can be more relevant during summertime due to drier soil conditions and higher atmospheric
 336 turbulence. Moreover, the good correlation between these elements (Al vs Si: $R^2=0.94$ and Ca vs Si: $R^2=0.78$) suggested
 337 the common origin.

338 Potassium was the element showing the most different median concentrations in the two seasons; its median concentration
 339 in low time resolution samples was 284 ng m^{-3} (10th-90th percentile: $151\text{-}344 \text{ ng m}^{-3}$) and 660 ng m^{-3} (10th-90th percentile:
 340 $349\text{-}982 \text{ ng m}^{-3}$) in summer and winter, respectively. K is an ambiguous tracer, since it is emitted by a variety of sources
 341 such as crustal resuspension and biomass burning. In our dataset, wintertime K values showed a good correlation with
 342 levoglucosan concentrations ($R^2=0.71$) suggesting an impact of wood biomass burning as levoglucosan is a well-known
 343 tracer for biomass burning emissions in winter samples (Simoneit et al., 1999). Also looking at K-to-Si ratio (the latter taken
 344 as soil dust marker) significant seasonal differences came out; it was 0.35 ± 0.15 in high time resolution summer samples
 345 and 2.0 ± 2.2 in winter ones, to be compared with the much more stable ratio for Al/Si (i.e. 0.26 ± 0.04 and 0.28 ± 0.09
 346 in summer and winter, respectively).

347 Among the elements typically associated to anthropogenic sources, Fe and Cu showed a good correlation (e.g. $R^2=0.72$
 348 on hourly resolution samples) as well as Cu and EC (Cu vs EC: $R^2=0.84$, on low time resolution data). In addition, the
 349 diurnal pattern of Fe and Cu showed traffic rush-hours peaks (7-9 a.m. and around 19 p.m. as shown in Fig.1). These
 350 results were suggestive of a common source. Indeed, these aerosol chemical components are reported in the literature as
 351 tracers for vehicular emissions (e.g. Viana et al., 2008; Thorpe and Harrison, 2008).



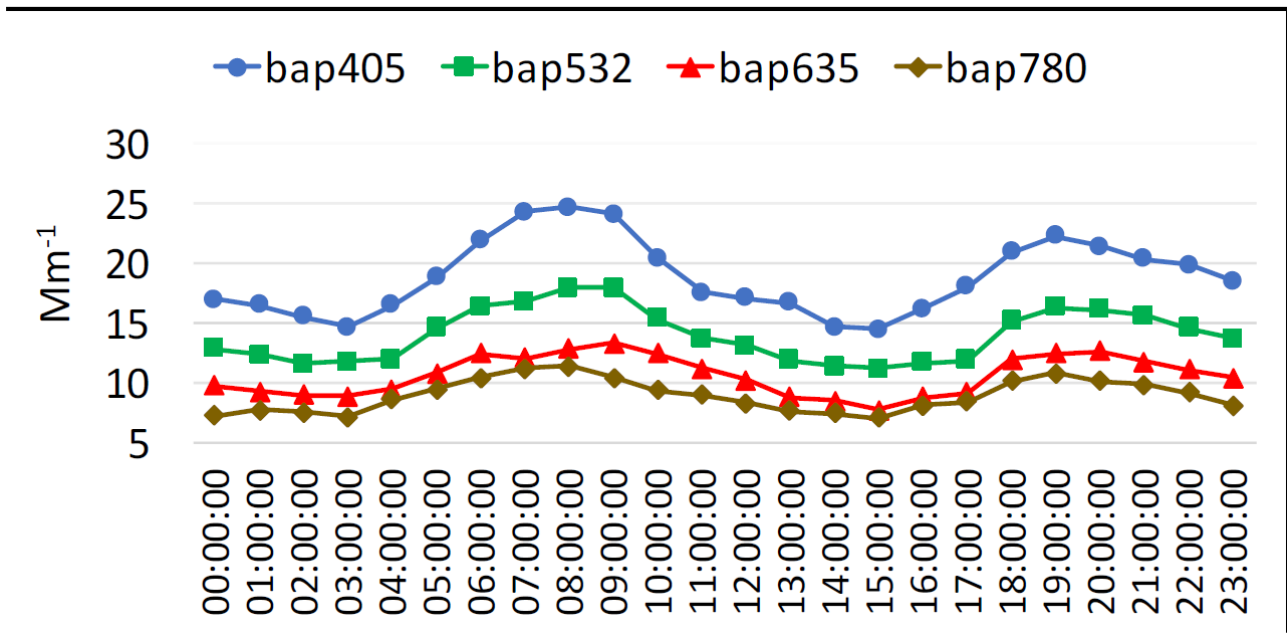
352

353 Figure 1: Diurnal profile of Fe and Cu concentrations (in ng m^{-3}).

354

355 In Table S2 (Supplement) also basic statistics on b_{ap} values referred to low resolution samples collected on PTFE are
356 reported. Diurnal mean temporal patterns for b_{ap} at different wavelengths (retrieved from hourly resolved data) ~~is~~are
357 displayed in Fig. 2.

358



359

360 Figure 2: Diurnal profile of aerosol absorption coefficient measured at different wavelengths.

361

362 3.2 Source apportionment with ~~multi-time~~ multi-time resolution model

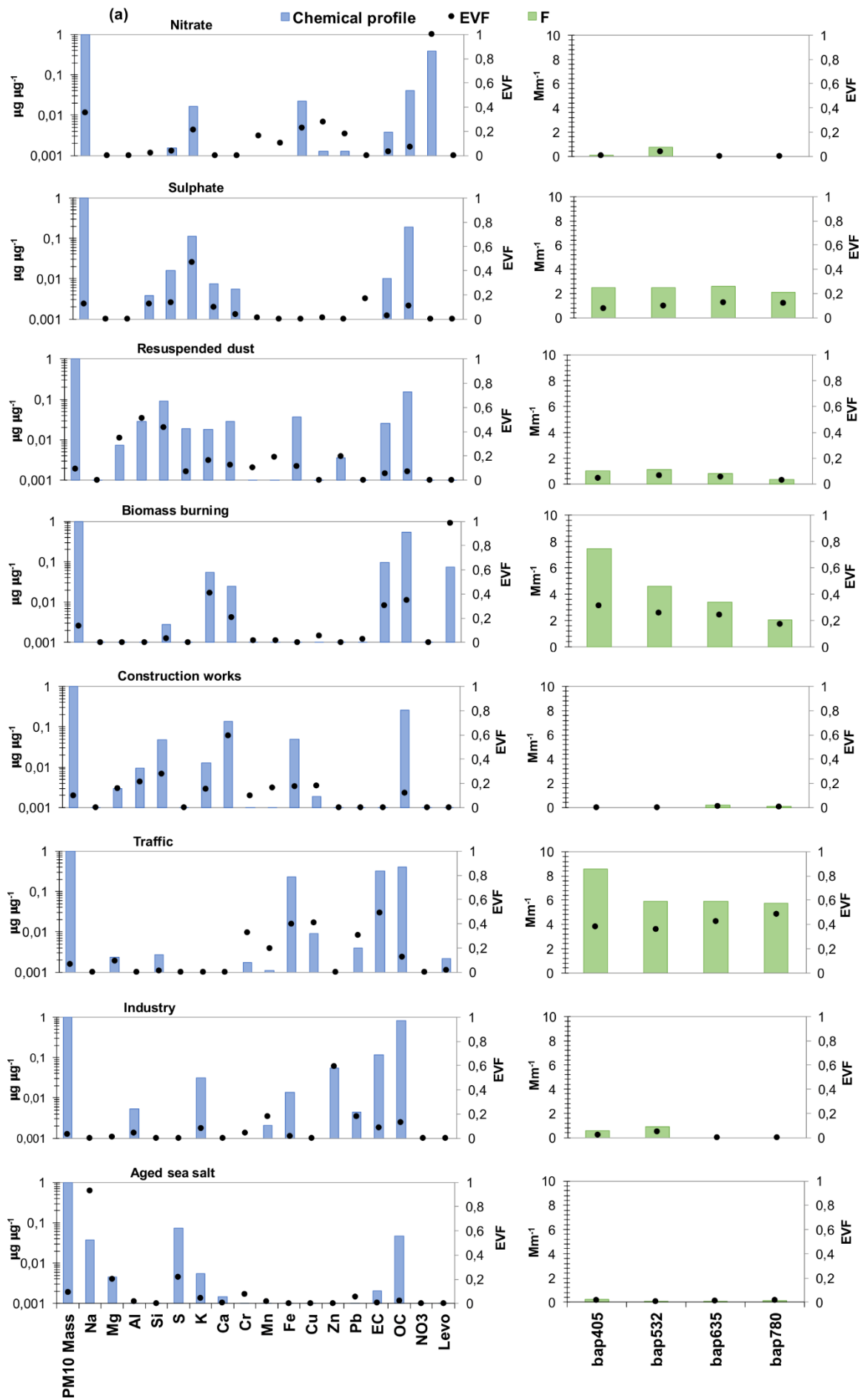
363 Different number of factors (5-10) were explored; after 30 convergent runs, ~~an~~the 8-factor base-case solution
364 corresponding to the lowest Q value (2086.88) was firstly selected (see Fig. S1 in the Supplement). It is important to
365 notice that the model was run using all variables (chemical + optical) as explained in Sect. 2.5. A lower or higher number
366 of factors caused ambiguous chemical profiles ~~and~~ the physical interpretation ~~highlighted~~ singled out clearly mixed
367 sources for a lower number of factors or unique factors in case of more factors (i.e. Pb for 9 factors); moreover,
368 inconsistent mass closure was detected increasing the number of factors (e.g. the sum of species contribution was up to
369 25 % higher than the mass for the 10-factor solution). In the 8-factor base case solution, the mass was well reconstructed
370 by the model ($R^2=0.98$), with a slope of 0.98 ± 0.02 and negligible intercept= $0.51 \pm 0.89 \mu\text{g m}^{-3}$.

371 The factor-to-source assignment process was based on both the Explained Variation for F matrix (~~FVEVF~~) values - which
372 are typically higher for chemical tracers (Lee et al., 1999; Paatero, 2010) - and the physical consistence of factor chemical
373 profiles. In the chosen solution, the not explained variation was lower than 0.25 for all variables. The scaled residuals

374 showed a random distribution of negative and positive values in the ± 3 range, [with a Gaussian shape for most of the](#)
375 [variables \(Fig. S2 in the Supplement\).](#)

376 Using ~~EVEVF~~ and chemical profiles reported in Fig. S1(a), the 8 factors were tentatively assigned to specific atmospheric
377 aerosol sources: nitrate, sulphate, resuspended dust, biomass burning, construction works, traffic, industry, and aged sea
378 salt. In Table [S3](#) (in the Supplement) absolute and relative average source contributions to PM10 mass are reported.

379 Although the above mentioned base-case solution was a satisfactory representation of the main sources active in the area
380 (as reported in previous works, see e.g. Marcazzan et al., 2003; Vecchi et al., 2009 and 2018; Bernardoni et al., 2011 and
381 2017a; Amato et al., 2016), the chemical profiles of some factors ~~could be~~ improved exploring rotated solutions. The
382 most relevant case was represented by aged sea-salt where typical diagnostic ratios such as Mg/Na and Ca/Na were not
383 well reproduced (in bulk sea water equal to 0.12 and 0.04, respectively, as reported e.g. in Seinfeld and Pandis, 2006) and
384 the chemical profile itself was too much impacted by the presence of Fe compared to bulk sea water composition.
385 Therefore, the above-mentioned diagnostic ratios were here used as constraints and Fe was maximally pulled down in the
386 chemical profile. The effective increase in Q was of about 61 units (Q=2147), with a percentage increase of about 3 ~~%~~
387 ~~%~~; as a rule of thumb, an increase in the Q value of a few tens is generally [considered](#) acceptable (Paatero and Hopke,
388 2009). It is noteworthy that an improvement in the chemical profiles was achieved with negligible differences—, compared
389 to the base-case solution —as for all other relevant features of the solution (i.e. ~~EVEVF~~, residuals, mass reconstruction,
390 source apportionment). Therefore, ~~an~~ [the](#) 8-factor constrained solution was considered the most physically reliable; results
391 are presented in Table 1 and Fig. [3](#) and discussed in detail in the following.



393 Figure 3: (a) Chemical profiles of the 8-factor constrained solution (b) b_{ap} apportionment of the 8-factor constrained
 394 solution.

395

Factors	Summer [$\mu\text{g m}^{-3}$]	Winter [$\mu\text{g m}^{-3}$]	Total [$\mu\text{g m}^{-3}$]
Nitrate	3.6 (15 %)	21.1 (44 %)	10.2 (31 %)
Sulphate	6.3 (26 %)	8.1 (17 %)	7.0 (21 %)
Resuspended dust	4.6 (19 %)	1.7 (4 %)	3.5 (11 %)
Biomass burning	0.32 (1 %)	8.3 (17 %)	3.3 (10 %)
Construction works	5.9 (24 %)	3.4 (7 %)	4.9 (15 %)
Traffic	1.4 (6 %)	2.2 (5 %)	1.7 (5 %)
Industry	0.86 (4 %)	1.2 (3 %)	1.0 (3 %)
Aged sea salt	1.4 (6 %)	1.8 (4 %)	1.6 (5 %)

396 Table 1: Absolute and relative average source contributions to PM10 mass in the 8-factor constrained solution.

397

398 The factor interpreted as nitrate fully accounted for the explained variation of NO_3^- . This factor ~~contains~~ contained a
 399 significant fraction of nitrate in the chemical profile (39 %) and all nitrate ~~is accounted~~ was present for only in this
 400 factor. This source ~~is~~ was by large the most significant ~~source~~ one at the investigated site, ~~accounting for~~ explaining about
 401 31 % of the PM10 mass over the whole campaign (a similar estimate – 26 % - was reported by Amato et al. (2016)
 402 during the AIRUSE campaign in Milan in 2013) raising up to 44 % during wintertime (comparable to 37 % reported
 403 by Vecchi et al. (2018)). Indeed, the Po valley is well-known for experiencing very high nitrate concentrations during
 404 wintertime (Vecchi et al., 2018; and references therein) because of large emissions of gaseous precursors related to urban
 405 and industrial activities, ~~wood~~ biomass burning used for residential heating, high ammonia levels due to agricultural fields
 406 manure and – last but not the least – poor atmospheric dispersion conditions.

407 The factor associated to sulphate shows $\text{EVF}=0.47$ for S and much lower EVF for all the other variables in the factor.
 408 ~~which contributes to the chemical profile for about 11%~~ Considering the contribution of S in the chemical profile in terms
 409 of sulphate and ammonium sulphate as e.g. Marcazzan et al. (2004), the relative contribution of sulphur components in the
 410 profile increases from 11% (S) up to 45% (ammonium sulphate). The latter is the main sulphur compound detected
 411 in the Po valley as reported in previous papers such as e.g. Marcazzan et al. (2001) and was by far the highest contributor
 412 in the chemical profile. The other important contributor was OC (19%), whose impact on PM mass increased up to
 413 30% when reported as organic matter using 1.6 as the organic carbon-to-organic matter conversion factor for this site
 414 (Vecchi et al., 2004) (corresponding to 33% as SO_4^{2-} and 45% as ammonium sulphate). Due to the secondary origin of
 415 the aerosol associated to this factor, it ~~is~~ was not surprising to find also a significant OC contribution ~~(19%)~~; indeed, ~~as~~
 416 ~~already pointed out for the same location by Vecchi et al. (2018), in Milan aerosol chemical composition in Milan is~~
 417 impacted by highly oxygenated components due to aging processes favoured by strong atmospheric stability (Vecchi et
 418 al., 2018 and 2019). In this factor, EC contributeed for about 1%. Considering the total EC concentration reconstructed

419 ~~by the model, the EC fraction related to the sulphate factor was about 6%.~~ Opposite to sulphates, EC has a primary
420 ~~origin; however, its presence with a very similar percentage (4-5%) in a sulphate chemical profile has been~~
421 ~~already previously pointed out highlighted in Milan, indicating a more complex mixing between primary and secondary~~
422 ~~sources (Amato et al., 2016). The sulphate factor accounts-accounted for 21% of the PM10 mass.~~
423 ~~The factor identified as re-suspended dust is mainly characterised by high EVs and contributions coming from Al, Si and~~
424 ~~Mg, i.e. crustal elements. The Al/Si ratio is 0.31, very similar to the literature value for average crust composition (Mason,~~
425 ~~1966); the relatively high contribution of OC in the chemical profile (15%) and the presence of EC (about 2.6%),~~
426 ~~indicate that there is very likely a mixing with road dust (Thorpe and Harrison, 2008). This source accounts for about 11~~
427 ~~% of the PM10 mass.~~
428 The factor identified as biomass burning ~~is-was~~ characterised by high EVF for levoglucosan (0.98), a known tracer for
429 this source as it is generated by cellulose pyrolysis; EVF higher than 0.3 ~~are-were~~ also found for K, OC, and EC. In the
430 source chemical profile, OC ~~contributes-contributed~~ for 54%, EC for 10%, levoglucosan for 7%, and K for 5%
431 %. The average biomass burning contribution during this campaign ~~is-was~~ 10% (up to 17% in wintertime).
432 Anticipating the discussion presented in detail in Sect. 3.3, it is worth noticing that ~~in this factor there is also~~ the second
433 largest contribution to the aerosol absorption coefficient after traffic was detected in this factor.
434 The factor with high (0.60) EVF (0.60) for Ca ~~is-was~~ associated to construction works, following literature works (e.g.
435 Vecchi et al., 2009; Bernardoni et al., 2011; Dall'Osto, 2013; Crilley et al., 2017; Bernardoni et al., 2017a; and references
436 therein). Major contributors to the chemical profile ~~were~~ Ca (13%), OC (26%), Fe, and Si (5% each). This factor
437 ~~accounts-accounted~~ on average for 15% to PM10 mass. As already mentioned, during the campaign a not negligible
438 contribution from this source ~~could-be-was~~ expected, due to the presence of a construction building site nearby the
439 monitoring location.
440 In the factor here assigned to traffic (primary contribution), ~~EVF~~ EVF larger than 0.3 ~~are-found-fcharacterised or~~ EC, Cu,
441 Fe, Cr, and Pb. The highest relative contributions in terms of mass in the chemical profile ~~are-were~~ given by OC (41%
442 %), EC (32%), Fe (23%), and Cu (1%). ~~The lack of important-relevant~~ crustal elements such as Ca and Al in the
443 ~~chemical profile, suggest-ed a negligible that the impact of road dust is negligible in this factor. Indeed, as already~~
444 ~~pointed-out-reported above, at our sampling site the road dust contribution was very likely mixed in the to resuspended~~
445 ~~dust- and further separation of these contributions was not possible-factor. The OC to EC ratio is about 1.3 which is~~
446 ~~consistent with a primary traffic contribution (Giugliano et al., 2005; Bernardoni et al., 2011).~~ This traffic (primary)
447 contribution over the whole dataset ~~accounts-accounted~~ for 5% of the PM10 mass with a slightly lower absolute
448 contribution in summer (see Table 1). This contribution is comparable to the percentage (7%) reported by Amato et
449 al. (2016) for exhaust traffic emissions but it is lower than our previous estimates (Bernardoni et al., 2011; Vecchi et al.,

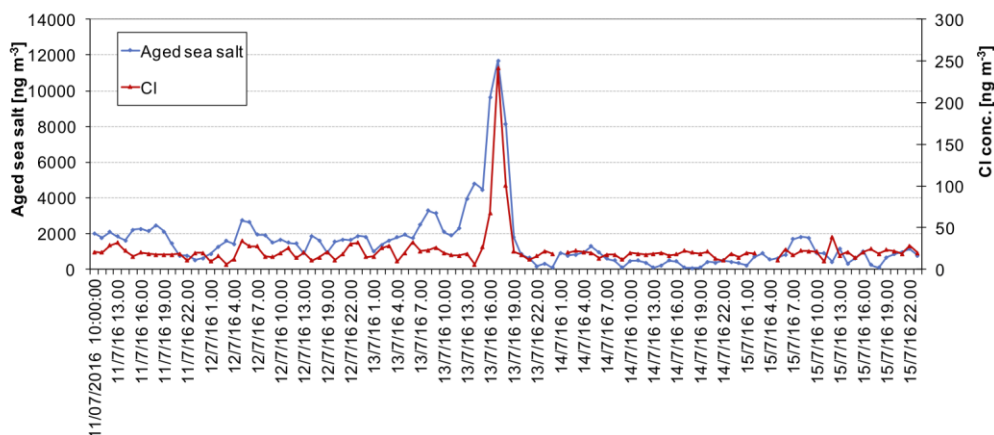
450 ~~2018~~, i.e. 15 % in 2006 in PM10 and 12 % in PM1 recorded in winter 2012, ~~as reported in Bernardoni et al. (2011)~~
451 ~~and Vecchi et al. (2018), respectively~~. However, the current estimate seems to be still reasonable when considering the
452 efforts done in latest years to reduce vehicles exhaust particle emissions and the fraction of secondary nitrate to be added
453 to account for the overall traffic impact; indeed, a significant traffic contribution due to nitrate should be accounted for
454 the relevant nitrogen oxides and ammonia emissions from agriculture in the region (INEMAR ARPA-Lombardia, 2018).
455 Unfortunately, the non-linearity of the emission-to-ambient concentration levels relationship and the high uncertainties
456 in emission inventories still prevent a robust estimate of this secondary contribution to total traffic exhaust emissions. In
457 Sect. 3.3, it will be shown that traffic is the largest contributor to aerosol absorption coefficient, a result that reinforces
458 the interpretation of this factor as a traffic emission source.

459 The industry factor ~~shows~~ showed high ~~EVEVF~~ for Zn (0.59) ~~and~~ and the second highest ~~EVEVF~~ ~~is~~ was related to Mn
460 (0.13). Previous studies at the same sampling site identified these elements as tracers for industrial emissions (e.g. Vecchi
461 et al., 2018; and references therein). The chemical profile ~~is~~ resulted enriched by heavy metals and, after traffic, it ~~is~~ was
462 the profile with the highest share of Cr, Mn, Fe, Cu, Zn, and Pb (explaining about 8 % of the total PM10 mass in the
463 profile). The industry contribution ~~is~~ was not very high in the urban area of Milan, accounting for 3 % on average.

464 The factor interpreted as aged sea salt ~~has~~ was characterised by high ~~EVEVF~~ of Na (0.93) and this element ~~is~~ was - as a
465 matter of fact - present only in this factor chemical profile. To check the physical consistency of this assignment and
466 considering that Milan is about 120 km away from the nearest sea coast, back-trajectories coloured by the aged sea salt
467 concentration (in ng m⁻³) frequencies were calculated through the NOAA HYSPLIT trajectory model (Draxler and Hess,
468 1998; Stein et al., 2015; Rolph et al., 2017) and represented using the Openair software (Carslaw and Ropkins, 2012).
469 When marine air masses are transported to polluted sites, sea salt particles are characterised by a Cl deficit due to reactions
470 with sulphuric and nitric acid (Seinfeld and Pandis, 2006). In this case, the factor chemical profile was expected to be
471 enriched in sulphate and nitrate. In this work, nitrate was not present; a very rough estimate (Lee et al., 1999) gave a
472 maximum expected contribution of 2 % (about 82 ng m⁻³) of the total nitrate mass in atmosphere, that can be considered
473 negligible in terms of mass contribution of the sources.

474 ~~F.30~~ Temporal patterns of Cl concentrations (not inserted in the ~~multi-time~~ multi-time resolution analysis as being a weak
475 variable) during episodes were exploited to further confirm the factor-to-source association. As an example, a very short
476 event (13/07 h. 16-18) ~~highlighted~~ singled out by the model and representing the highest sea salt contribution during
477 summer ~~is~~ was here analysed in further detail. Before and during the sea salt event, air masses ~~showed a clear~~
478 ~~origin~~ originated from south-west compatible with Ligurian sea while soon after the event, there was a rapid change of
479 wind direction (Fig. S243, in the Supplement). These hours were characterised by an average high wind speed of $4.8 \pm$
480 1.7 m s^{-1} (with a maximum peak of 9.5 m s^{-1}) compared to $1.9 \pm 1.0 \text{ m s}^{-1}$ average wind speed recorded during the summer

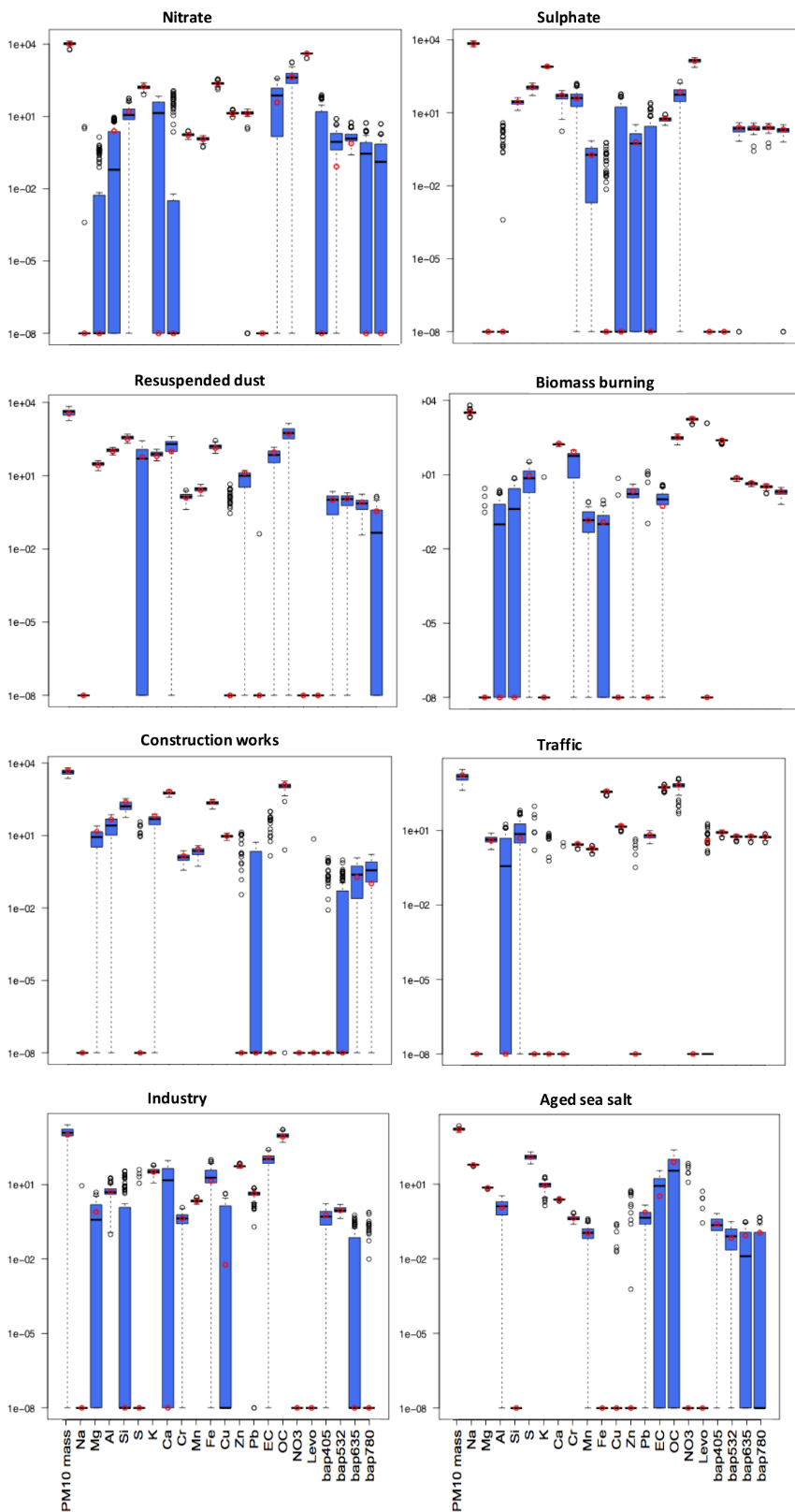
481 campaign. In addition, Cl concentration and aged sea salt pattern showed an evident temporal coincidence in peak
 482 occurrence during the event (Fig. 4), thus ~~confirming the correctness of supporting~~ the source identification. ~~In~~
 483 ~~addition~~ Moreover, ~~d~~ During this episode, only the Cl coarse fraction increased (Fig. S4, in the Supplement) and reached
 484 about 90 % of total PM10 Cl concentration; Cl/Na ratio was 0.38 ± 0.05 , consistent with an aging of marine air masses
 485 during advection showing the typical Cl depletion due to the interaction between sea salt particles and polluted air masses
 486 (Seinfeld and Pandis, 2006).



487
 488 Figure 4: Temporal patterns of aged sea salt source retrieved from the ~~multi-time~~ multi-time resolution model and Cl
 489 concentrations measured in ~~atmosphere~~ atmospheric aerosol.

490
 491 **DISCUSSION**

492 Bootstrap analysis was performed to evaluate the uncertainties associated to source profiles (Crespi et al., 2016). 100 runs
 493 were carried out (see Fig. 5, values expressed in ng m^{-3} or Mm^{-1} on a logarithmic scale); factors were well mapped, with
 494 Pearson coefficient always higher than 0.97, and tracers for each source showed small interquartile range, supporting the
 495 goodness of the solution presented in this work.



496

497

498

499

Figure 35: Box plot of the bootstrap analysis on the 8-factor constrained solution. The red dots represent the output values of the solution of the model; the black lines the medians from the bootstrap analysis; the blue bars the 25th and 75th percentile; the dotted lines the interval equal to 1.5 the interquartile range and the black dots the outliers from this interval.

500

501 *3.3 Improving source apportionment with optical tracers*

502 First of all, the use of the absorption coefficient determined at different wavelengths as input variable in the ~~multi-~~
503 ~~time~~multi-time resolution model, strengthened the identification of the sources, suggesting that it can be exploited when
504 specific chemical tracers are not available (e.g. levoglucosan for ~~wood~~biomass burning). To prove that, a separate source
505 apportionment study was performed with EPA PMF 5.0 (Norris et al., 2014), introducing only hourly elemental
506 concentrations from samples collected by the streaker sampler and hourly b_{ap} at different λ measured by PP_UniMI on
507 the same filters. Streaker samples typically lack of a complete chemical characterisation; in particular, important chemical
508 tracers such as levoglucosan and EC are not available. In this analysis, b_{ap} assessed at different wavelengths resulted
509 particularly useful for the identification of the biomass burning factor that explained a significant percentage of the b_{ap}
510 itself (from 25 ~~%~~ % to 35 ~~%~~ % depending on λ) (Fig. S5, in the Supplement); without this additional information, the
511 factor-to-source assignment would be otherwise based only on the presence of elemental potassium ~~while being~~although
512 it is well-known that ~~potassium-K~~ cannot be considered an unambiguous tracer as it is emitted by a variety of sources (see
513 for example Pachon et al., 2013; and references therein). Furthermore,

514 ~~As for the multi-time~~multi-time resolution model, results showed that the absorption coefficient contribution was higher
515 than 45 ~~%~~ % in the factor labelled as traffic, highlighting the importance of exhaust emissions in a factor that would be
516 otherwise characterised mainly on elements related to non-exhaust emissions (Cu, Fe, Cr).

517 ~~From the multi-time resolution model,~~Furthermore, the two factors identified as biomass burning and traffic ~~are~~were the
518 main contributors to aerosol absorption in atmosphere and showed significant ~~EVEVF~~ values. Contributions to b_{ap}
519 ~~were~~Traffic accounts for 55 % of b_{ap} at 780 nm and 42 % at 405 nm for traffic and ; biomass burning accounts for
520 20 % and 36 % for biomass burning at 780 and 405 nm, respectively. The Explained Variation (~~EVEVF~~) of b_{ap} has
521 the maximum value at 405 nm for biomass burning (0.32) and at 780 nm for traffic (0.49), showing the tendency to
522 decrease and increase with the wavelength, respectively.

523 The third contributor to aerosol absorption in atmosphere ~~was~~ the sulphate factor, with a contribution comparable to the
524 biomass burning one at 780 nm (about 20% of the total reconstructed b_{ap} at this wavelength). The sulphate factor
525 contains a small fraction of EC, as previously discussed (see Sect. 3.2). This might be explained considering that
526 non/weakly light-absorbing material can form a coating that can enhance absorption (Bond and Bergstrom, 2006; Fuller
527 et al., 1999) within a few days after emission (Bond et al., 2006)~~This might be explained considering that ionic compounds~~
528 ~~can condense on light absorbing carbon particles, forming a coating of negligibly absorbing material that can enhance~~
529 ~~absorption (Bond & Bergstrom, 2006; Fuller et al., 1999) within a few days after emission (Bond et al., 2006).~~ Laboratory
530 experiments and simulations from in-situ measurements highlighted absorption amplification for absorbing particles

531 coated with secondary organic aerosol (Schnaiter et al., 2003; Moffet and Prather, 2009). These processes related to
532 particles aging can become important in the Po valley due to low atmospheric dispersion conditions and they might
533 explain the higher-relatively high contribution of the sulphate factor to the absorption coefficient in respect to the other
534 sources (excluding traffic and biomass burning). Among the other sources, resuspended dust ~~was~~ the main contributor at
535 all wavelengths (between 3% % and 7% % of the total reconstructed b_{ap} , depending on the wavelength), ~~highlighting~~
536 ~~probably the likely due to the role of iron minerals. The other four sources ~~were~~ less relevant in terms of EVF values~~
537 and overall contributed for less than 11% %.

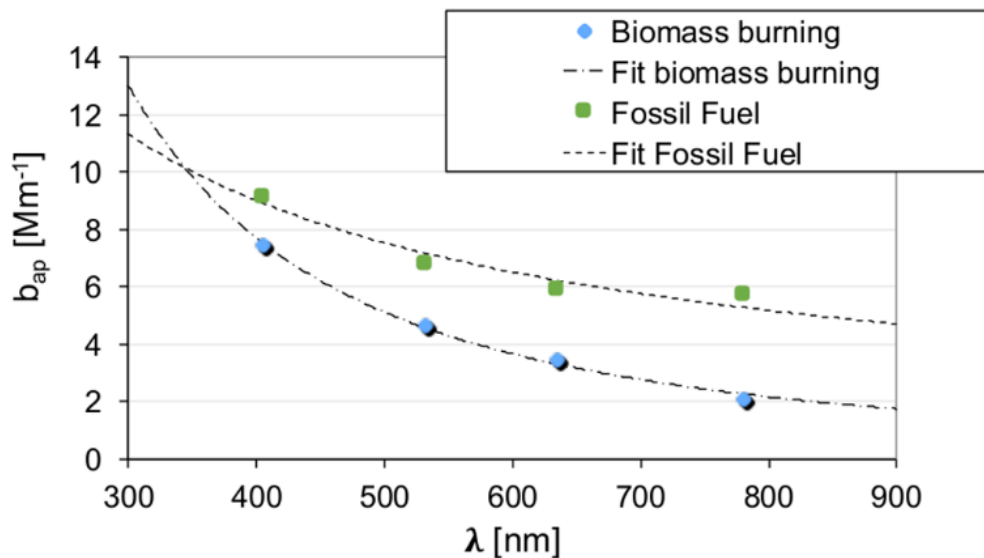
538

539 ~~The other six sources are less relevant in terms of EV values and overall contribute for less than 30%.~~

540 It is noteworthy that opposite to the approach used in source apportionment optical models, like the widespread
541 Aethalometer model (Sandradewi et al., 2008a) and MWAA model (Massabò et al., 2015; Bernardoni et al., 2017b), no
542 a-priori information about the Absorption Ångström Exponent (α) of the fossil fuel and biomass burning sources was
543 introduced in the ~~multi-time~~multi-time resolution model; instead, an estimate for its value ~~can be~~was directly retrieved
544 from the ~~obtained solution~~model. It has to be mentioned that optical models are typically based on a two-source hypothesis
545 (i.e. biomass burning and fossil fuel emissions); an exception reported in previous works (Wang et al., 2011) concerned
546 the use of Delta-C used as an input variable together with chemical aerosol components in source apportionment models
547 and proved to be very effective in separating traffic (especially diesel) emissions from ~~wood~~biomass combustion
548 emissions.

549 ~~It has to be mentioned that optical models are based on a two-source hypothesis (i.e. biomass burning and fossil fuel~~
550 ~~emissions).~~ Hereafter, in order to compare ~~multi-time~~multi-time resolution model and optical models results,
551 contributions due to traffic and industry (i.e. emissions most likely connected to fossil fuel usage) were added up and
552 labelled as “fossil fuel emissions”. Similarly to the two-source approach used in the Aethalometer model, in the following,
553 the discussion about optical properties will be hereafter focused on the biomass burning and fossil fuel sources ,
554 considering that sulphate and resuspended dust factors ~~were~~ less significant also in terms of EVF for optical variables,
555 ranging from 0.08 to 0.12 and from 0.03 and 0.06, respectively, depending on the wavelength.

556 In Fig. 6 the wavelength dependence of b_{ap} for the biomass burning and the fossil fuel profiles obtained with the ~~multi-~~
557 ~~time~~multi-time resolution model is shown; as α values can show significant differences when calculated using different
558 pairs of λ (Sandradewi et al., 2008b), here we performed a ~~the~~ fitting procedure considering $b_{ap} \propto \lambda^{-\alpha}$. Results were,
559 gives α_{BB} (α biomass burning) = 1.83 and α_{FF} (α fossil fuels) = 0.80; ~~The bootstrap analysis allowed to estimate the~~
560 range of variability of α values ~~was estimated with the bootstrap analysis obtaining, considering the 25th and 75th~~
561 percentile: 0.78-0.88 for α_{FF} and 1.65-1.88 for α_{BB} (as 25th and 75th percentile, respectively).



562

563 Figure 6: b_{ap} dependence on λ for biomass burning and fossil fuel emissions.

564

565 ~~The value of α_{BB} value obtained in this work is very similar to 1.86 found for biomass burning by Sandradewi et al.~~
 566 ~~(2008a) and 1.8 obtained by Massabò et al. (2015) who used also independent ¹⁴C measurements for checking.~~

567 ~~The α_{FF} value (assumed to be equal to α_{BC} in source apportionment optical models) obtained in this work is in the range~~
 568 ~~0.8-1.1 typically reported in optical source apportionment studies (e.g. Bernardoni et al., 2017b; and references therein).~~

569 ~~It is also consistent with the atmospheric α value obtained during the summer campaign, when biomass burning was~~
 570 ~~negligible (impacting 1 % of the total PM10 mass from the multi-time source apportionment). Zotter et al. (2017)~~

571 ~~considered different sampling sites in Switzerland (urban, rural, traffic and background) and they found reported a possible~~
 572 ~~combination of $\alpha_{FF}=0.8$ and $\alpha_{BB}=1.8$ when EC concentration from fossil fuel combustion (estimated with radiocarbon~~

573 ~~measurements) is between 40% and 85% of the total EC concentration; in this work, the fraction of EC ascribed by~~
 574 ~~the multi-time model to fossil fuel sources was 56%. In the same work,~~

575 ~~The assessment of α_{BC} (assumed to be equal to α_{FF} in source apportionment optical models) is still an issue and both~~
 576 ~~experimental and simulation studies are in progress to reduce uncertainties and give a better evaluation of this relevant~~

577 ~~optical parameter.~~

578 ~~The α_{BB} value retrieved by the model was very similar to values reported by Zotter et al. (2017) and also comparable to~~
 579 ~~1.86 found for biomass burning by Sandradewi et al. (2008a) and 1.8 obtained by Massabò et al. (2015) who used also~~

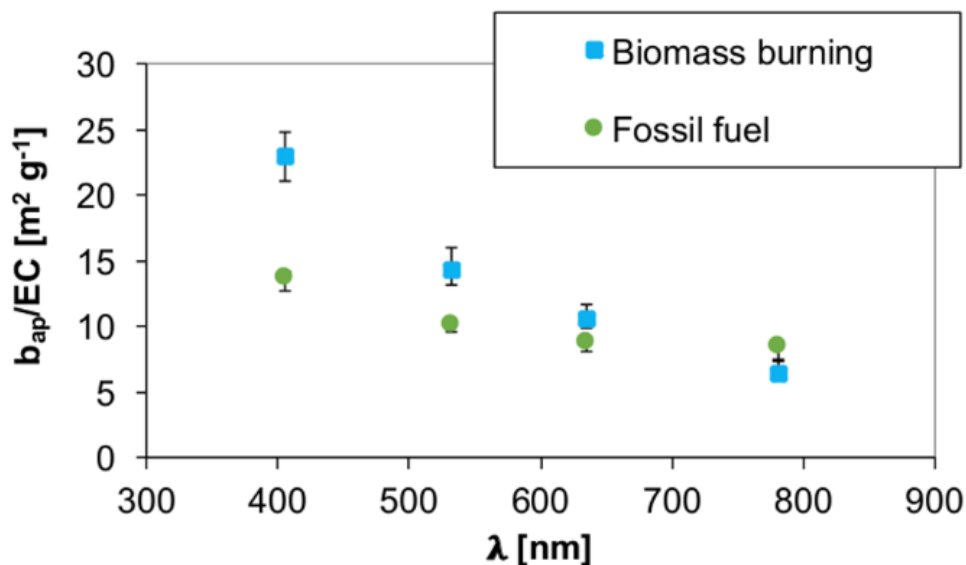
580 ~~independent ¹⁴C measurements for checking. The α_{FF} value (assumed to be equal to α_{BC} in source apportionment optical~~
 581 ~~models) resulted in the range 0.8-1.1 typically reported in optical source apportionment studies (e.g. Bernardoni et al.,~~

582 ~~2017b; Zotter et al., 2017; and references therein). Indeed, the sampling site was an urban background station in Milan~~

583 where aerosol aging is a relevant process and our samples hardly had been impacted by fresh traffic emissions.
584 Considering this feature of Milan aerosol, the average α_{FF} was included in the wide range of estimates for BC coated
585 particles reported in literature works (approx. 0.6-1.3, see e.g. Liu et al., 2018) and obtained by both ambient measurement
586 (e.g. Fischer and Smith, 2018; and references therein) and numerical simulations (e.g. Gyawali et al., 2009; Liu et al.
587 2018; and references therein).

588 Results here reported allow also to study the relationship between the absorption coefficient and the mass of black carbon,
589 i.e. the so called Mass Absorption Cross section (MAC) at different wavelengths. The $MAC(\lambda) = b_{ap}(\lambda)/BC$ relationship
590 assumes that black carbon (BC) is the only light-absorbing species present; however, this assumption is not always valid,
591 since mineral dust and brown carbon (BrC) can significantly contribute to aerosol absorption. During our monitoring
592 campaign, no significant contribution from mineral dust was observed; opposite, biomass burning was proved to be a
593 relevant source so that BrC was certainly a significant contributor (Fuzzi et al., 2015) as also suggested by $\alpha_{BB} = 1.83$ in
594 the biomass burning factor. The possible overestimation of BC when total b_{ap} is ascribed to BC only is usually minimised
595 choosing a wavelength higher than 600 nm, exploiting the spectral dependence of absorption from different aerosol
596 compounds (Petzold et al., 2013).

597 EC concentration retrieved from the chemical profiles (see Fig. 3) was used as a proxy for BC to estimate source-
598 dependent $b_{ap}(\lambda)$ -to-BC ratio. Results are represented in Fig. 7. It is noteworthy that here this ratio is intentionally not
599 indicated as MAC, since overestimation of the BC absorption especially at lower λ might occur (see previous discussion).
600 BrC is expected to give a small contribution in the fossil fuel source; therefore, the best approximation for $MAC(\lambda)$ values
601 are likely the $b_{ap}(\lambda)$ -to-BC ratios observed in the fossil fuel source at our monitoring site. They resulted to be $13.7 \text{ m}^2 \text{ g}^{-1}$
602 at $\lambda = 405 \text{ nm}$; $10.2 \text{ m}^2 \text{ g}^{-1}$ at $\lambda = 532 \text{ nm}$; $8.8 \text{ m}^2 \text{ g}^{-1}$ at $\lambda = 635 \text{ nm}$; $8.6 \text{ m}^2 \text{ g}^{-1}$ at $\lambda = 780 \text{ nm}$. At $\lambda = 550 \text{ nm}$ Bond and
603 Bergstrom (2006) report $MAC = 7.5 \pm 1.2 \text{ m}^2 \text{ g}^{-1}$ for uncoated fresh emitted particles and MAC values in polluted regions
604 ranging from 9 to $12 \text{ m}^2 \text{ g}^{-1}$, attributable to absorption enhancement due to particles coating. The MAC estimate obtained
605 in this work from ~~multi-time~~ multi-time resolution model at 532 nm is comparable to literature values and it confirms the
606 importance of aging processes in atmosphere on the optical properties of particles.



607

608 Figure 7: b_{ap} -to-EC ratio dependence on λ for biomass burning and fossil fuel emissions. Error bars represent the 25th and
 609 75th percentile retrieved from the bootstrap analysis.

610

611 Ratios in Fig. 7 are ~~clearly~~ less comparable at $\lambda=405$ nm (see also [Table S34, in the Supplement](#)) ~~due to the , this result~~
 612 ~~is explained by the~~ significant contribution of BrC to b_{ap} at this wavelength in the biomass burning factor.

613 No seasonal differences in the atmospheric ratios were observed but at $\lambda = 405$ nm (see [Table S34, in the Supplement](#)),
 614 for which winter values are higher than summer ones (17.8 ± 0.4 and 14.2 ± 0.5 , respectively); this result can be explained
 615 considering the influence of biomass burning emissions on BrC concentration in atmosphere during the winter season.

616 From the outputs of the modelling approach here proposed, the apportionment of the biomass burning and fossil fuel
 617 contributions to b_{ap} at different wavelengths was also obtained. As expected, the relative contribution to the total
 618 reconstructed b_{ap} ascribed to the biomass burning factor decreases with increasing λ , opposite to the contribution from
 619 fossil fuel combustion which gives the highest contribution at 780 nm ([Table 2](#)); in addition, the latter contribution prevails
 620 at all wavelengths at the investigated site.

	$\lambda = 405 \text{ nm}$	$\lambda = 532 \text{ nm}$	$\lambda = 635 \text{ nm}$	$\lambda = 780 \text{ nm}$
Biomass burning	36 % (31 %-36 %)	29 % (25 %-30 %)	26 % (23 %-27 %)	20 % (16 %-22 %)
Fossil fuels	45 % (41 %-46 %)	43 % (39 %-44 %)	45 % (41 %-47 %)	55 % (48 %-55 %)

Table 2: Average contribution to total reconstructed b_{ap} for the biomass burning and fossil fuel factors; in parenthesis 25th and 75th percentile are reported.

621

622 4. Conclusions

623 The ~~multi-time~~multi-time resolution model implemented through Multilinear Engine (ME2) script allowed the analysis
624 of experimental data collected at different time scales, coupling the detailed chemical speciation at low time resolution
625 and the temporal information given by high time resolution samples. The effect of the introduction of the aerosol
626 absorption coefficient (b_{ap}) measured at different wavelengths in the modelling process was investigated and gave
627 promising results. First of all, a more robust identification of sources was provided; secondly, it paved the way to the
628 retrieval of optical apportionment and optical characterisation of the sources (e.g. estimate of source-specific Absorption
629 Ångström Exponent - α - and MAC at different wavelengths). It is worthy to note that – at the state of the art – in source
630 apportionment optical models (e.g. Aethalometer model) values for α related to fossil fuel emissions and ~~wood~~biomass
631 burning are fixed by the modeller thus carrying a large part of the uncertainties in the model results. Considering that the
632 estimates for the Absorption Ångström Exponent were here obtained as a result of a quite complex modelling approach
633 (i.e. using multi-time resolution datasets collected on limited periods) and without any a-priori assumption, the results
634 obtained – although obviously affected by a certain degree of uncertainty due to both experimental data and modelling
635 process (here estimated while typically not taken into consideration for fixed α values used in the literature) – were fairly
636 comparable to literature results and gave a further tool aimed at assessing more robust source-related α values. In
637 perspective, joining together different approaches such as the receptor modelling here proposed and e.g. ^{14}C
638 measurements and artefact-free b_{ap} measurements will lead to better estimates of the Absorption Ångström Exponent;
639 work is in progress at our laboratories to achieve this goal.

640 The original approach described in this work can be applied to any source apportionment study using any suitable dataset
641 (not necessarily with multi-time resolution). Besides the traditional source apportionment, the impact of different sources
642 on the aerosol absorption coefficient was estimated; this piece of information can be very useful to formulate strategies
643 of pollutants abatement, in order to improve air quality and to face climate challenges. In particular, at the investigated
644 site secondary compounds constituted the highest contribution in terms of PM10 mass (52 % on average), while the

645 two factors identified as biomass burning and traffic were found to be the most significant contributors to aerosol
646 absorption in atmosphere, in agreement with available literature works.

647

648 **Acknowledgements**

649 This work was partially funded by the Italian National Institute of Nuclear Physics under the INFN experiments
650 DEPOTMASS and TRACCIA. ACTRIS-IT funded the publication of the paper. The authors thank Prof. Paola Fermo
651 (Dept. of Chemistry, University of Milan) for availability of the Sunset instrument to perform EC/OC analyses and ARPA
652 – Lombardia for meteorological data availability. The mechanical workshop of the Dept. of Physics – University of Milan
653 is gratefully acknowledged for the realisation of parts of the polar photometer. The authors ~~acknowledge also ARPA~~
654 ~~Lombardia for meteorological data availability~~ are grateful to Prof. Philip Hopke for hints on multi-time resolution ME-
655 2.

656

657 **Data availability.**

658 The data in the study are available from the authors upon request (roberta.vecchi@unimi.it).

659

660 **Supplement.**

661 The supplement related to this article is available online

662

663 **Author contributions.**

664 ACF performed streaker sampling and related optical analysis, implemented the advanced model, analysed the results,
665 and drafted the paper. GV contributed to model implementation, ~~and~~ data reduction and Hysplit back-trajectories retrieval.
666 VB, SV, and REP carried out the sampling campaign on filters, performed the optical measurements and data analysis.
667 GC, SN, and FL performed PIXE analysis and data reduction. DM and PP carried out ionic characterisation on filters and
668 data analysis. RV was responsible for the design and coordination of the study, the synthesis of the results and the final
669 version of the paper. All authors contributed to the interpretation of the results obtained with the new approach here
670 described and revised the manuscript content giving a final approval of the version to be submitted. RV and ACF reviewed
671 the paper addressing reviewers' comments.

672

673

674 **Competing interests.**

675 The authors declare that they have no conflict of interest.

676

677

678 **References**

679 Amato F., Alastuey A., Karanasiou A., Lucarelli F., Nava S., Calzolari G., Severi M., Becagli S., Gianelle V.N., Colombi
680 C., Alves C., Custódio D., Nunes T., Cerqueira M., Pio C., Eleftheriadis K., Diapouli E., Reche C., Minguillón M.C.,
681 Manousakas M.I., Maggos T., Vratolis S., Harrison R.M. and Querol X.: AIRUSE-LIFE+: a harmonized PM speciation
682 and source apportionment in five southern European cities, *Atmos. Chem. Phys.*, 16, 3289-3309,
683 <https://doi.org/10.5194/acp-16-3289-2016>, 2016.

684

685 Andreae M.O. and Gelencsér A.: Black carbon or brown carbon? The nature of light-absorbing carbonaceous aerosols,
686 *Atmos. Chem. Phys.*, 6, 3131-3148, <https://doi.org/10.5194/acp-6-3131-2006>, 2006.

687

688 Belis C.A., Larsen B.R., Amato F., El Haddad I., Favez O., Harrison R.M., Hopke P.K., Nava S., Paatero P., Prévot A.,
689 Quass U., Vecchi R. and Viana M.: European Guide on Air Pollution Source Identification with Receptor Models,
690 Luxembourg: Publications Office of the European Union, Joint Research Center – Institute for Environment and
691 Sustainability, European Union, <https://doi.org/10.2788/9332>, 2014.

692 Belis C.A., Karagulian F., Amato F., Almeida M., Artaxo P., Beddows D.C.S., Bernardoni V., Bove M.C., Carbone S.,
693 Cesari D., Contini D., Cuccia E., Diapouli E., Eleftheriadis K., Favez O., El Haddad I., Harrison R.M., Hellebust S.,
694 Hovorka J., Jang E., Jorquera H., Kammermeier T., Karl M., Lucarelli F., Mooibroek D., Nava S., Nøjgaard J.K., Paatero
695 P., Pandolfi M., Perrone M.G., Petit J.E., Pietrodangelo A., Pokorná P., Prati P., Prevot A.S.H., Quass U., Querol X.,
696 Saraga D., Sciare J., Sfetsos A., Valli G., Vecchi R., Vestenius M., Yubero E. and Hopke P.K.: A new methodology to
697 assess the performance and uncertainty of source apportionment models II: The results of two European intercomparison
698 exercises, *Atmos. Environ.*, 123, 240-250, <https://doi.org/10.1016/j.atmosenv.2015.10.068>, 2015.

699

700 Bernardoni V., Vecchi R., Valli G., Piazzalunga A. and Fermo P.: PM10 source apportionment in Milan (Italy) using
701 time-resolved data, *Sci. Total Environ.*, 409, 4788-4795, <https://doi.org/10.1016/j.scitotenv.2011.07.048>, 2011.

702 Bernardoni V., Elser M., Valli G., Valentini S., Bigi A., Fermo P., Piazzalunga A. and Vecchi R.: Size-segregated
703 aerosol in a hot-spot pollution urban area: Chemical composition and three-way source apportionment, *Environ. Pollut.*,
704 231, 601-611, <https://doi.org/10.1016/j.envpol.2017.08.040>, 2017a.

705

706 Bernardoni V., Pileci R.E., Caponi L. and Massabò D.: The Multi-Wavelength Absorption Analyzer (MWAA) model as

707 a tool for source and component apportionment based on aerosol absorption properties: application to samples collected
708 in different environments, *Atmosphere*, 8, 218, <https://doi.org/10.3390/atmos8110218>, 2017b.

709 Bernardoni V., Valli G. and Vecchi R.: Set-up of a multi-wavelength polar photometer for the off-line measurement of
710 light absorption properties of atmospheric aerosol collected with high-temporal resolution, *J. Aerosol. Sci.*, 107, 84-93,
711 <https://doi.org/10.1016/j.jaerosci.2017.02.009>, 2017c.

712 Bigi A. and Ghermandi G.: Long-term trend and variability of atmospheric PM₁₀ concentration in the Po Valley, *Atmos.*
713 *Chem. Phys.*, 14, 4895-4907, <https://doi.org/10.5194/acp-14-4895-2014>, 2014.

714 Bond T.C. and Bergstrom R.W.: Light absorption by carbonaceous particles: an investigative review, *Aerosol Sci. Tech.*,
715 40, 27-67, <https://doi.org/10.1080/02786820500421521>, 2006.

716 Bond T.C., Doherty S.J., Fahey D.W., Forster P.M., Berntsen T., DeAngelo B.J., Flanner M.G., Ghan S., Kärcher B.,
717 Koch D., Kinne S., Kondo Y., Quinn P.K., Sarofim M.C., Schultz M.G., Schulz M., Venkataraman C., Zhang H., Zhang
718 S., Bellouin N., Guttikunda S.K., Hopke P.K., Jacobson M.Z., Kaiser J.W., Klimont Z., Lohmann U., Schwarz J.P.,
719 Shindell D., Storelvmo T., Warren S.G. and Zender C.S.: Bounding the role of black carbon in the climate system: A
720 scientific assessment, *J. Geophys. Res.-Atmos.*, 118, 5380-5552, <https://doi.org/10.1002/jgrd.50171>, 2013.

721 Brown S.G., Eberly S., Paatero P. and Norris G.A.: Methods for estimating uncertainty in PMF solutions: Examples with
722 ambient air and water quality data and guidance on reporting PMF results, *Sci. Total Environ.*, 518-519, 626-635,
723 <https://doi.org/10.1016/j.scitotenv.2015.01.022>, 2015.

724 Calzolari G., Chiari M., Lucarelli F., Mazzei F., Nava S., Prati P., Valli G. and Vecchi R.: PIXE and XRF analysis of
725 particulate matter samples: an inter-laboratory comparison, *Nucl. Instrum. Meth. B*, 266, 2401-2404,
726 <https://doi.org/10.1016/j.nimb.2008.03.056>, 2008.

727 Calzolari G., Lucarelli F., Chiari M., Nava S., Giannoni M., Carraresi L., Prati P. and Vecchi R.: Improvements in PIXE
728 analysis of hourly particulate matter samples, *Nucl. Instrum. Meth. B*, 363, 99-104,
729 <https://doi.org/10.1016/j.nimb.2015.08.022>, 2015.

730 [Cappa C.D., Lack D.A., Burkholder J.B., and Ravishankara A.R.: Bias in filter-based aerosol light absorption](#)
731 [measurements due to organic aerosol loading: Evidence from laboratory measurements. *Aerosol Sci. Tech.*, 42, 1022-](#)
732 [1032, <https://doi.org/10.1080/02786820802389285>, 2008.](#)

733 [Carslaw D.C. and Ropkins K.: Openair — an R package for air quality data analysis. *Environ. Modell. Softw.* 27/28,](#)
734 [52-61, <https://doi.org/10.1016/j.envsoft.2011.09.008>, 2012](#)

735 Crespi A., Bernardoni V., Calzolari G., Lucarelli F., Nava S., Valli G. and Vecchi R.: Implementing constrained multi-
736 time approach with bootstrap analysis in ME-2: an application to PM_{2.5} data from Florence (Italy), *Sci. Total Environ.*,
737 541, 502-511, <https://doi.org/10.1016/j.scitotenv.2015.08.159>, 2016.

738 Crilley L.R., Lucarelli F., Bloss W.J., Harrison R.M., Beddows D.C., Calzolari G., Nava S., Valli G., Bernardoni V. and
739 Vecchi R.: Source Apportionment of Fine and Coarse Particles at a Roadside and Urban Background Site in London
740 during the Summer ClearLo Campaign, *Environ. Pollut.*, 220, 766-778, <https://doi.org/10.1016/j.envpol.2016.06.002>,
741 2017.

742 D'Alessandro A., Lucarelli F., Mandò P.A., Marcazzan G., Nava S., Prati P., Valli G., Vecchi R. and Zucchiatti A.:
743 Hourly elemental composition and sources identification of fine and coarse PM10 particulate matter in four Italian towns,
744 *J. Aerosol Sci.*, 34, 243-259, [https://doi.org/10.1016/S0021-8502\(02\)00172-6](https://doi.org/10.1016/S0021-8502(02)00172-6), 2003.

745 Dall'Osto, M., Querol, X., Amato, F., Karanasiou, A., Lucarelli, F., Nava, S., Calzolari, G. and Chiari, M.: Hourly
746 elemental concentrations in PM2.5 aerosols sampled simultaneously at urban background and road site during SAPUSS
747 e diurnal variations and PMF receptor modelling, *Atmos. Chem. Phys.*, 13, 4375-4392, [https://doi.org/10.5194/acp-13-](https://doi.org/10.5194/acp-13-4375-2013)
748 [4375-2013](https://doi.org/10.5194/acp-13-4375-2013), 2013.

749 [Davies N.W., Fox C., Szpek K., Cotterell M.I., Taylor J.W., Allan J.D., Williams P.I., Trembath J., Haywood j.M., and](#)
750 [Langridge J.M: Evaluating biases in filter-based aerosol absorption measurements using photoacoustic spectroscopy,](#)
751 [Aerosol Meas. Tech., 12, 3417–3434, <https://doi.org/10.5194/amt-12-3417-2019>, 2019.](#)

752 Draxler R.R. and Hess G.D.: An overview of the HYSPLIT_4 modelling system for trajectories, dispersion, and
753 deposition, *Aust. Meteorol. Mag.*, 47, 295-308, 1998.

754 Fialho P., Hansen A.D.A. and Honrath R.E.: Absorption coefficients by aerosols in remote areas: a new approach to
755 decouple dust and black carbon absorption coefficients using seven-wavelength Aethalometer data, *J. Aerosol Sci.*, 36,
756 267-282, <https://doi.org/10.1016/j.jaerosci.2004.09.004>, 2005.

757 Fischer D.A. and Smith G.D.: A portable, four wavelength, single-cell photoacoustic spectrometer for ambient aerosol
758 absorption, *Aerosol Sci. Tech.*, 52, 393-406, <https://doi.org/10.1080/02786826.2017.1413231>, 2018.

759 Fuzzi S., Baltensperger U., Carslaw K., Decesari S., Denier van der Gon H., Facchini M.C., Fowler D., Koren I., Langford
760 B., Lohmann U., Nemitz E., Pandis S., Riipinen I., Rudich Y., Schaap M., Slowik J.G., Spracklen D.V., Vignati E., Wild
761 M., Williams M. and Gilardoni S.: Particulate matter, air quality and climate: lessons learned and future needs, *Atmos.*
762 *Chem. Phys.*, 15, 8217-8299, <https://doi.org/10.5194/acp-15-8217-2015>, 2015.

763 ~~Giugliano M., Lonati G., Butelli P., Romele L., Tardivo R. and Grosso M.: Fine particulate (PM2.5-PM1) at urban sites~~
764 ~~with different traffic exposure, *Atmos. Environ.*, 39, 2421–2431, <https://doi.org/10.1016/j.atmosenv.2004.06.050>, 2005.~~

765 Gyawali M., Arnott W.P., Lewis K. and Moosmüller H.: In situ aerosol optics in Reno, NV, USA during and after the
766 summer 2008 California wildfires and the influence of absorbing and non-absorbing organic coatings on spectral light
767 absorption, *Atmos.Chem.Phys.*, 9, 8007-8015, <https://doi.org/10.5194/acp-9-8007-2009>, 2009.

768 Hennigan C.J., Sullivan A.P., Collett J.L.Jr and Robinson A.L.: Levoglucosan stability in biomass burning particles

769 exposed to hydroxyl radicals, *Geophys. Res. Lett.*, 37, 9, <https://doi.org/10.1029/2010GL043088>, 2010.

770 Henry R.C.: History and fundamentals of multivariate air quality receptor models, *Chemometr. Intell. Lab.*, 37, 37-42,
771 [https://doi.org/10.1016/S0169-7439\(96\)00048-2](https://doi.org/10.1016/S0169-7439(96)00048-2), 1997.

772 Hopke P.K.: Review of receptor modeling methods for source apportionment, *J. Air Waste Manage.*, 66, 3, 237-259,
773 <https://doi.org/10.1080/10962247.2016.1140693>, 2016.

774 INEMAR - ARPA Lombardia: INEMAR, Inventario Emissioni in Atmosfera: emissioni in Regione Lombardia nell'anno
775 2014 - dati finali, ARPA Lombardia Settore Monitoraggi Ambientali,
776 <http://www.inemar.eu/xwiki/bin/view/Inemar/HomeLombardia>, 2018.

777 IPCC: Climate Change 2013: The Physical Science Basis. Contribution of Working Group I to the Fifth Assessment
778 Report of the Intergovernmental Panel on Climate Changes, Stocker T.F., Qin D., Plattner G.-K., Tignor M., Allen S.K.,
779 Boschung J., Nauels A., Xia Y., Bex V. and P.M. Midgley, Cambridge University Press, Cambridge, United Kingdom
780 and New York, NY, USA, <https://doi.org/10.1017/CBO9781107415324>, 2013.

781 Kim E., Hopke P.K. and Edgerton E.S.: Source identification of Atlanta aerosol by positive matrix factorization, *J. Air
782 Waste Manage.*, 53, 6, 731-739, <https://doi.org/10.1080/10473289.2003.10466209>, 2003.

783 Kuo C.-P., Liao H.-T., Chou C.C.-K. and Wu C.-F.: Source apportionment of particulate matter and selected volatile
784 organic compounds with multiple time resolution data, *Sci. Total Environ.*, 472, 880-887,
785 <https://doi.org/10.1016/j.scitotenv.2013.11.114>, 2014.

786 [Lack D.A., Cappa C.D., Covert D.S., Baynard T., Massoli P., Sierau B., Bates T.S., Quinn P.K., Lovejoy E.R., and
787 Ravishankara A.R.: Bias in filter-based aerosol light absorption measurements due to organic aerosol loading: Evidence
788 from ambient measurements. *Aerosol Sci. Tech.*, 42, 1033-1041, <https://doi.org/10.1080/02786820802389277>, 2008.](#)

789 Lee E., Chan C.K. and Paatero P.: Application of positive matrix factorization in source apportionment of particulate
790 pollutants in Hong Kong, *Atmos. Environ.*, 33, 3201-3212, [https://doi.org/10.1016/S1352-2310\(99\)00113-2](https://doi.org/10.1016/S1352-2310(99)00113-2), 1999.

791 Liao H.-T., Chou C.C.-K., Chow J.C., Watson J.G., Hopke P.K. and Wu C.-F.: Source and risk apportionment of selected
792 VOCs and PM_{2.5} species using partially constrained receptor models with multiple time resolution data, *Environ. Pollut.*,
793 205, 121-130, <https://doi.org/10.1016/j.envpol.2015.05.035>, 2015.

794 Liu C., Chung C.E., Yin Y. and Schnaiter M.: The absorption Ångström exponent of black carbon: from numerical
795 aspects. *Atmos. Chem. Phys.*, 18, 6259-6273, <https://doi.org/10.5194/acp-2017-836>, 2018.

796 Marcazzan G.M., Ceriani M., Valli G. and Vecchi R.: Source apportionment of PM₁₀ and PM_{2.5} in Milan (Italy) using
797 receptor modelling, *Sci. Total Environ.*, 317, 137-147, [https://doi.org/10.1016/S0048-9697\(03\)00368-1](https://doi.org/10.1016/S0048-9697(03)00368-1), 2003.

798 Mason B.: Principles of geochemistry, 3rd Edition, John Wiley & Sons, New York, 1966.

799 Massabò D., Caponi L., Bernardoni V., Bove M.C., Brotto P., Calzolari G., Cassola F., Chiari M., Fedi M.E., Fermo P.,

800 Giannoni M., Lucarelli F., Nava S., Piazzalunga A., Valli G., Vecchi R. and Prati P.: Multi-wavelength optical
801 determination of black and brown carbon in atmospheric aerosols, *Atmos. Environ.*, 108, 1-12,
802 <https://doi.org/10.1016/j.atmosenv.2015.02.058>, 2015.

803 Massabò D., Caponi L., Bove M.C. and Prati P.: Brown carbon and thermal-optical analysis: A correction based on optical
804 multi-wavelength apportionment of atmospheric aerosols, *Atmos. Environ.*, 125, 119-125,
805 <https://doi.org/10.1016/j.atmosenv.2015.11.011>, 2016.

806 Norris G., Duvall R., Brown S. and Bai S.: EPA Positive Matrix Factorization (PMF) 5.0. Fundamentals and User Guide,
807 U.S. Environmental Protection Agency, Washington, DC, 2014.

808 Ogulei D., Hopke P.K., Zhou L., Paatero P., Park S.S. and Ondov J.M.: Receptor modeling for multiple time resolved
809 species: the Baltimore supersite, *Atmos. Environ.*, 39, 3751-3762, <https://doi.org/10.1016/j.atmosenv.2005.03.012>, 2005.

810 Paatero P.: Least squares formulation of robust non-negative factor analysis, *Chemometr. Intell. Lab.*, 37, 23-35,
811 [https://doi.org/10.1016/S0169-7439\(96\)00044-5](https://doi.org/10.1016/S0169-7439(96)00044-5), 1997.

812 Paatero P.: The Multilinear Engine – A Table-drive least squares program for solving multilinear problems, including the
813 n-way parallel factor analysis model, *J. Comput. Graph. Stat.*, 8, 4, 854-888,
814 <https://doi.org/10.1080/10618600.1999.10474853>, 1999.

815 Paatero P.: User's guide for the Multilinear Engine program "ME2" for fitting multilinear and quasi-multilinear models,
816 University of Helsinki, Department of Physics, Finland, 2000.

817 Paatero P.: User's Guide for Positive Matrix Factorization programs PMF2 and PMF3, Part 2: reference, available
818 www.helsinki.fi/~paatero/PMF/pmf2.zip (PMFDOC2.pdf), last update 2010.

819 Paatero P.: The Multilinear Engine (ME-2) script language (v. 1.352), available with the program ME-2 (me2scrip.txt).
820 2012.

821 Paatero P.: User's guide for positive matrix factorization programs PMF2 and PMF3, part 1: Tutorial, available at
822 www.helsinki.fi/~paatero/PMF/pmf2.zip (PMFDOC1.pdf), last update 2015.

823 [Paatero P.: Interactive comment on a paper submitted to ACPD, available at https://doi.org/10.5194/acp-2018-784-RC2,](https://doi.org/10.5194/acp-2018-784-RC2)
824 [2018](https://doi.org/10.5194/acp-2018-784-RC2)

825 Paatero P. and Hopke P.K.: Rotational tools for factor analytic models. *J. Chemometr.*, 23, 91-100,
826 <https://doi.org/10.1002/cem.1197>, 2009.

827 Paatero P. and Tapper U.: Positive Matrix Factorization: a non-negative factor model with optimal utilization of error
828 estimates of data values, *Environmetrics*, 5, 111-126, <https://doi.org/10.1002/env.3170050203>, 1994.

829 Pachon J.E., Weber R.J., Zhang X., Mulholland J.A. and Russell A.G.: Revising the use of potassium (K) in the source
830 apportionment of PM_{2.5}, *Atmos. Pollut. Res.*, 4, 14-21, <https://doi.org/10.5094/APR.2013.002>, 2013.

831 [Peré-Trepat E., Kim E., Paatero P. and Hopke P.K.: Source apportionment of time and size resolved ambient particulate](#)
832 [matter measured with a rotating DRUM impactor, Atmos. Environ., 41, 5921-5933,](#)
833 [https://doi.org/10.1007/s11356-013-2067-1](https://doi.org/10.1016/j.atmosenv.2007.03.022, 2007.</p><p>834 Perrino C., Catrambone M., Dalla Torre S., Rantica E., Sargolini T. and Canepari S.: Seasonal variations in the chemical
835 composition of particulate matter: a case study in the Po Valley. Part I: macro-components and mass closure, Environ.
836 Sci. Pollut. Res., 21, 3999-4009, <a href=), 2014.

837 Perrone M.G., Larsen B.R., Ferrero L., Sangiorgi G., De Gennaro G., Udisti R., Zangrando R., Gambaro A. and
838 Bolzacchini E.: Sources of high PM_{2.5} concentrations in Milan, Northern Italy: Molecular marker data and CMB
839 modelling. Sci. Total Environ., 414, 343-355, <https://doi.org/10.1016/j.scitotenv.2011.11.026>, 2012.

840 Petzold A., Ogre J.A., Fiebig M., Laj P., Li S.-M., Baltensperger U., Holzer-Popp T., Kinne S., Pappalardo G., Sugimoto
841 N., Wehrli C., Wiedensohler A. and Zhang X.-Y.: Recommendations for the interpretation of “black carbon”
842 measurements, Atmos. Chem. Phys., 13, 8365-8379, <https://doi.org/10.5194/acp-13-8365-2013>, 2013.

843 Piazzalunga A., Fermo P., Bernardoni V., Vecchi R., Valli G. and De Gregorio M.A.: A simplified method for
844 levoglucosan quantification in wintertime atmospheric particulate matter by high performance anion-exchange
845 chromatography coupled with pulsed amperometric detection, Int. J. Environ. Anal. Chem., 90, 934-947,
846 <https://doi.org/10.1080/03067310903023619>, 2010.

847 Piazzalunga A., Bernardoni V., Fermo P., Valli G. and Vecchi R. Technical note: On the effect of water-soluble
848 compounds removal on EC quantification by TOT analysis in urban aerosol samples, Atmos. Chem. Phys., 11, 10193-
849 10203, <https://doi.org/10.5194/acp-11-10193-2011>, 2011.

850 Piazzalunga A., Bernardoni V., Fermo P. and Vecchi R.: Optimisation of analytical procedures for the quantification of
851 ionic and carbonaceous fractions in the atmospheric aerosol and application to ambient samples, Anal. Bioanal. Chem.,
852 405, 1123-1132, <https://doi.org/10.1007/s00216-012-6433-5>, 2013.

853 Polissar A., Hopke P.K., Paatero P., Malm W.C. and Sisler J.F.: Atmospheric aerosol over Alaska: elemental composition
854 and sources. J. Geophys. Res. 103, 19045-19057, <https://doi.org/10.1029/98JD01212>, 1998.

855 Pope III C.A. and Dockery D.W.: Health effects of fine particulate air pollution: lines that connect, J. Air Waste Manage.,
856 56, 709-742, <https://doi.org/10.1080/10473289.2006.10464485>, 2006.

857 Robinson A.L., Donahue N.M. and Rogge W.F.: Photochemical oxidation and changes in molecular composition of
858 organic aerosol in the regional context, J. Geophys. Res., 111, D3, <https://doi.org/10.1029/2005JD006265>, 2006.

859 Rolph G., Stein A. and Stunder B.: Real-time Environmental Application and Display sYstem: READY, Environ. Modell.
860 Softw., 95, 210-228, <https://doi.org/10.1016/j.envsoft.2017.06.025>, 2017.

861 Sandradewi J., Prévôt A.S.H., Szidat S., Perron N., Alfarra M.R., Lanz V.A., Weingartner E. and Baltensperger U.:

862 Using aerosol light absorption measurements for the quantitative determination of wood burning and traffic emission
863 contributions to particulate matter, *Environ. Sci. Technol.*, 42, 3316-3323, 2008a.

864 [Sandradewi J., Prévôt A.S.H., Weingartner E., Schmidhauser R., Gysel M. and Baltersperger U.: A study of wood](#)
865 [burning and traffic aerosols in an Alpine valley using a multi-wavelength Aethalometer, *Atmos. Environ.*, 2, 101–112,](#)
866 [doi:10.1016/j.atmosenv.2007.09.034, 2008b.](#)

867 Seinfeld J.H. and Pandis S.N.: Atmospheric chemistry and physics: from air pollution to climate change, 2nd edition, John
868 Wiley & Sons, INC, Hoboken, New Jersey, 2006.

869 [Simoneit B.R.: Levoglucosan, a tracer for cellulose in biomass burning atmospheric particles. *Atmos. Environ.*, 33, 173-](#)
870 [182, \[https://doi.org/10.1016/S1352-2310\\(98\\)00145-9\]\(https://doi.org/10.1016/S1352-2310\(98\)00145-9\), 1999.](#)

871

872 Sofowote U.M., Healy R.M., Su Y., Debozs J., Noble M., Munoz A., Jeong C.-H., Wang J.M., Hilker N., Evans G.J. and
873 Hopke P.K.: Understanding the PM_{2.5} imbalance between a far and near-road location: Results of high temporal frequency
874 source apportionment and parameterization of black carbon, *Atmos. Environ.*, 173, 277-288,
875 <https://doi.org/10.1016/j.atmosenv.2017.10.063>, 2018.

876 Stein A.F., Draxler R.R., Rolph G.D., Stunder B.J.B., Cohen M.D. and Ngan F.: NOAA's Hysplit atmospheric transport
877 and dispersion modeling system, *Bull. Am. Meteorol. Soc.*, 96, 2059-2077, [https://doi.org/10.1175/BAMS-D-14-](https://doi.org/10.1175/BAMS-D-14-00110.1)
878 [00110.1](#), 2015.

879 Thorpe A. and Harrison R.M.: Sources and properties of non-exhaust particulate matter from road traffic: A review, *Sci.*
880 *Total Environ.*, 400, 270-282, <https://doi.org/10.1016/j.scitotenv.2008.06.007>, 2008.

881 [Valentini S., Weber P., Bernardoni V., Bundke U., Massabò D., Petzold A., Prati P., Valli G. and Vecchi R.: Multi-](#)
882 [Wavelength Measurement of Aerosol Optical Properties: Laboratory Intercomparison of In-Situ and Filter-Based](#)
883 [Techniques, in Abstracts Book 12th International Conference on Carbonaceous Particles in the Atmosphere \(ICCPA\)](#)
884 [2019, 149, <https://iccpa2019.univie.ac.at/abstracts/>, 2019.](#)

885 Vecchi R., Marcazzan G., Valli G., Ceriani M. and Antoniazzi C.: The role of atmospheric dispersion in the seasonal
886 variation of PM₁ and PM_{2.5} concentration and composition in the urban area of Milan (Italy), *Atmos. Environ.*, 38, 4437–
887 4446, <https://doi.org/10.1016/j.atmosenv.2004.05.029>, 2004.

888 Vecchi R., Marcazzan G. and Valli G.: A study on nighttime-daytime PM₁₀ concentration and elemental composition in
889 relation to atmospheric dispersion in the urban area of Milan (Italy), *Atmos. Environ.*, 41, 2136-2144,
890 <https://doi.org/10.1016/j.atmosenv.2006.10.069>, 2007.

891 Vecchi R., Bernardoni V., Fermo P., Lucarelli F., Mazzei F., Nava S., Prati P., Piazzalunga A. and Valli G.: 4-hours
892 resolution data to study PM₁₀ in a “hot spot” area in Europe, *Environ. Monit. Assess.*, 154, 283–300,

893 <https://doi.org/10.1007/s10661-008-0396-1>, 2009.

894 [Vecchi R., Valli G., Fermo P., D'Alessandro A., Piazzalunga A., Bernardoni V.: Organic and inorganic sampling artefacts](#)

895 [assessment, Atmos. Environ., 43, 1713-1720, https://doi:10.1016/j.atmosenv.2008.12.016](#)

896 Vecchi R., Bernardoni V., Paganelli C. and Valli G.: A filter-based light absorption measurement with polar photometer:

897 effects of sampling artefacts from organic carbon, *J. Aerosol. Sci.*, 70, 15-25,

898 <https://doi.org/10.1016/j.jaerosci.2013.12.012>, 2014.

899 Vecchi R., Bernardoni V., Valentini S., Piazzalunga A., Fermo P. and Valli G.: Assessment of light extinction at a

900 European polluted urban area during wintertime: Impact of PM1 composition and sources, *Environ. Pollut.*, 233, 679-

901 689, <https://doi.org/10.1016/j.envpol.2017.10.059>, 2018.

902 Vecchi R., Piziali F.A., Valli G., Favaron M. and Bernardoni V.: Radon-based estimates of equivalent mixing layer

903 heights: A long-term assessment, *Atmos. Environ.*, 197, 150-158, <https://doi.org/10.1016/j.atmosenv.2018.10.020>, 2019.

904 Wang Y., Hopke P.K., Rattigan O.V., Xia X., Chalupa D.C. and Utell M.J.: Characterization of residential wood

905 combustion particles using the two-wavelength aethalometer, *Environ. Sci. Technol.*, 45, 7387-7393,

906 <https://doi.org/10.1021/es2013984>, 2011.

907 Wang Y., Hopke P.K., Rattigan O.V., Chalupa D.C. and Utell M.J.: Multiple-year black carbon measurements and source

908 apportionment using Delta-C in Rochester, New York, *J. Air Waste Manage.*, 62, 8, 880-887,

909 <https://doi.org/10.1080/10962247.2012.671792>, 2012.

910 Watson J.G.: Visibility: Science and Regulation, *J. Air Waste Manage.*, 52, 628-713,

911 <https://doi.org/10.1080/10473289.2002.10470813>, 2002.

912 Xie M., Chen X., Holder A.L., Hays M.D., Lewandowski M., Offenbergl J.H., Kleindienst T.E., Jaoui M. and Hannigan

913 M.P.: Light absorption of organic carbon and its sources at a southeastern U.S. location in summer, *Environ. Pollut.*, 244,

914 38-46, <https://doi.org/10.1016/j.envpol.2018.09.125>, 2019.

915 Yang M., Howell S.G., Zhuang J. and Huebert B.J.: Attribution of aerosol light absorption to black carbon, brown carbon,

916 and dust in China – interpretations of atmospheric measurements during EAST-AIRE, *Atmos. Chem. Phys.*, 9, 2035-

917 2050, <https://doi.org/10.5194/acp-9-2035-2009>, 2009.

918 Zhou L., Hopke P.K., Paatero P., Ondov J.M., Pancras J.P., Pekney N.J. and Davidson C.I.: Advanced factor analysis for

919 multiple time resolution aerosol composition data, *Atmos. Environ.*, 38, 4909-4920,

920 <https://doi.org/10.1016/j.atmosenv.2004.05.040>, 2004.

921 Zotter P., Herich H., Gysel M., El-Haddad I., Zhang Y., Mocnik G., Hüglin C., Baltensperger U., Szidat S. and Prévôt

922 A.S.H.: Evaluation of the absorption Ångström exponents for traffic and wood burning in the Aethalometer-based source

923 apportionment using radiocarbon measurements of ambient aerosol, *Atmos. Chem. Phys.*, 17, 4229-4249,

924 <https://doi.org/10.5194/acp-17-4229-2017>, 2017.

925

926

927

928

929 **List of Captions**

930 Figure 1: Diurnal profile of Fe and Cu concentrations (in ng m^{-3}).

931 Figure 2: Diurnal profile of the aerosol absorption coefficient measured at different wavelengths in Mm^{-1} .

932 Figure 3: (a) Chemical profiles of the 8-factor constrained solution (b) b_{ap} apportionment of the 8-factor constrained
933 solution.

934 Figure 4: Temporal patterns of aged sea salt source retrieved from the multi-time resolution model and Cl concentrations
935 measured in atmospheric aerosol.

936 Figure 5: Box plot of the bootstrap analysis on the 8-factor constrained solution. The red dots represent the output values
937 of the solution of the model; the black lines the medians from the bootstrap analysis; the blue bars the 25th and 75th
938 percentile; the dotted lines the interval equal to 1.5 the interquartile range and the black dots the outliers from this interval.

939 Figure 6: b_{ap} dependence on λ for biomass burning and fossil fuel emissions.

940 Figure 7: b_{ap} -to-EC ratio dependence on λ for biomass burning and fossil fuel emissions. Error bars represent the 25th and
941 75th percentile retrieved from the bootstrap analysis.

942

943 Table 1: Absolute and relative average source contributions to PM10 mass in the 8-factor constrained solution.

944 Table 2: Average contribution to total reconstructed b_{ap} for the biomass burning and fossil fuel factors; in parenthesis 25th
945 and 75th percentile are reported.

946 **List of Captions**

947 ~~Figure 1: Diurnal profile of the aerosol absorption coefficient measured at different wavelengths (upper panel); diurnal~~
948 ~~profile of Fe and Cu concentrations (in ng m^{-3}) (lower panel).~~

949 ~~Figure 2: Diurnal profile of the aerosol absorption coefficient measured at different wavelengths in Mm^{-1} .~~

950

951 ~~Figure 2: Hourly temporal patterns of Cu, K and aerosol absorption coefficient at 405 nm during an episode occurring on~~
952 ~~27th November.~~

953 ~~Figure 3: (a) Chemical profiles of the 8-factor constrained solution (b) b_{ap} apportionment of the 8-factor constrained~~

954 ~~solution.~~

955 ~~Figure 4: Temporal patterns of aged sea salt source retrieved from the multi-time resolution model and Cl concentrations~~
956 ~~measured in atmospheric aerosol.~~

957 ~~Figure 5: Box-plot of the bootstrap analysis on the 8-factor constrained solution. The red dots represent the output values~~
958 ~~of the solution of the model; the black lines the medians from the bootstrap analysis; the blue bars the 25th and 75th~~
959 ~~percentile; the dotted lines the interval equal to 1.5 the interquartile range and the black dots the outliers from this interval.~~

960 ~~Figure 6: b_{ap} dependence on λ for biomass burning and fossil fuel emissions.~~

961 ~~Figure 7: b_{ap} to EC ratio dependence on λ for biomass burning and fossil fuel emissions. Error bars represent the 25th and~~
962 ~~75th percentile retrieved from the bootstrap analysis.~~

963

964 ~~Table 1: Absolute and relative average source contributions to PM10 mass in the 8-factor constrained solution.~~

965 ~~Table 2: Average contribution to total reconstructed b_{ap} for the biomass burning and fossil fuel factors; in parenthesis~~
966 ~~25th and 75th percentile are reported.~~

967